Pergamon

Geochimica et Cosmochimica Acta, Vol. 68, No. 9, pp. 2167–2184, 2004

0016-7037/04 $30.00 + .00

doi:10.1016/j.gca.2003.10.025

Ca,Al-rich inclusions, amoeboid olivine aggregates, and Al-rich chondrules from the unique carbonaceous chondrite Acfer 094: I. Mineralogy and petrology

Alexander N. Krot,[1,*] Timothy J. Fagan,[2] Klaus Keil,[1] Kevin D. McKeegan,[3] Sandeep Sahijpal,[4] Ian D. Hutcheon,[5] Mikhail I. Petaev,[6] and Hisayoshi Yurimoto[2]

[1]Hawai'i Institute of Geophysics and Planetology, School of Ocean and Earth Science and Technology, University of Hawai'i at Manoa, Honolulu, HI 96822, USA
[2]Earth and Planetary Sciences, Tokyo Institute of Technology, Meguro, Tokyo 152-8551, Japan
[3]Department of Earth and Space Sciences, University of California, Los Angeles, CA 90095, USA
[4]Department of Physics, Panjab University, Chandigarh 160014, India
[5]Lawrence Livermore National Laboratory, Livermore, CA 94451, USA
[6]Harvard-Smithsonian Center for Astrophysics and Department of Earth and Planetary Sciences, Harvard University, Cambridge, MA 02138, USA

(*Received March* 6, 2003; *accepted in revised form October* 15, 2003)

Abstract—Based on their mineralogy and petrography, ~200 refractory inclusions studied in the unique carbonaceous chondrite, Acfer 094, can be divided into corundum-rich (0.5%), hibonite-rich (1.1%), grossite-rich (8.5%), compact and fluffy Type A (spinel-melilite-rich, 50.3%), pyroxene-anorthite-rich (7.4%), and Type C (pyroxene-anorthite-rich with igneous textures, 1.6%) Ca,Al-rich inclusions (CAIs), pyroxene-hibonite spherules (0.5%), and amoeboid olivine aggregates (AOAs, 30.2%). Melilite in some CAIs is replaced by spinel and Al-diopside and/or by anorthite, whereas spinel-pyroxene assemblages in CAIs and AOAs appear to be replaced by anorthite. Forsterite grains in several AOAs are replaced by low-Ca pyroxene. None of the CAIs or AOAs show evidence for Fe-alkali metasomatic or aqueous alteration. The mineralogy, textures, and bulk chemistry of most Acfer 094 refractory inclusions are consistent with their origin by gas-solid condensation and may reflect continuous interaction with SiO and Mg of the cooling nebula gas. It appears that only a few CAIs experienced subsequent melting. The Al-rich chondrules (ARCs; >10 wt% bulk Al_2O_3) consist of forsteritic olivine and low-Ca pyroxene phenocrysts, pigeonite, augite, anorthitic plagioclase, ± spinel, FeNi-metal, and crystalline mesostasis composed of plagioclase, augite and a silica phase. Most ARCs are spherical and mineralogically uniform, but some are irregular in shape and heterogeneous in mineralogy, with distinct ferromagnesian and aluminous domains. The ferromagnesian domains tend to form chondrule mantles, and are dominated by low-Ca pyroxene and forsteritic olivine, anorthitic mesostasis, and Fe,Ni-metal nodules. The aluminous domains are dominated by anorthite, high-Ca pyroxene and spinel, occasionally with inclusions of perovskite; have no or little FeNi-metal; and tend to form cores of the heterogeneous chondrules. The cores are enriched in bulk Ca and Al, and apparently formed from melting of CAI-like precursor material that did not mix completely with adjacent ferromagnesian melt. The inferred presence of CAI-like material among precursors for Al-rich chondrules is in apparent conflict with lack of evidence for melting of CAIs that occur outside chondrules, suggesting that these CAIs were largely absent from chondrule-forming region(s) at the time of chondrule formation. This may imply that there are several populations of CAIs in Acfer 094 and that mixing of "normal" CAIs that occur outside chondrules and chondrules that accreted into the Acfer 094 parent asteroid took place after chondrule formation. Alternatively, there may have been an overlap in the CAI- and chondrule-forming regions, where the least refractory CAIs were mixed with Fe-Mg chondrule precursors. This hypothesis is difficult to reconcile with the lack of evidence of melting of AOAs which represent aggregates of the least refractory CAIs and forsterite grains.

1. INTRODUCTION

Acfer 094 is a unique, type 3 carbonaceous chondrite breccia with mineralogical, petrologic, nitrogen isotopic and oxygen isotopic affinities to the CM and CO groups (Newton et al., 1995; Greshake, 1997). Its bulk chemical composition is similar to that of CM chondrites, whereas oxygen isotopic composition and matrix modal abundance are similar to those of CO chondrites. In contrast to CM chondrites, Acfer 094 shows no evidence for aqueous alteration and thermal metamorphism and has a distinctive carbon isotopic composition. Acfer 094 also has one of the highest abundances of presolar SiC and diamonds (Newton et al., 1995; Gao et al., 1996). In spite of these primitive characteristics, no systematic mineralogical and/or isotopic studies of chondrules and CAIs from this meteorite have been made so far (Weber et al., 1995; Krot et al., 1999; Hutcheon et al., 2000). Weber (1995) reported that the abundance of CAIs in Acfer 094 is < 2 vol%; their sizes range from 40 to 500 μm; secondary phases, such as nepheline, sodalite, and grossular are absent; the most common type of CAIs are Type A (melilite- and spinel-rich); and the CAIs are mineralogically and petrographically similar to those in CO and CR chondrites. Krot et al. (1999) described the mineralogy, oxygen and magnesium isotopic compositions of a relict spinel-hibonite CAI inside a ferromagnesian chondrule from Acfer 094. Hutcheon et al. (2000) reported excesses of ^{26}Mg ($^{26}Mg^*$) corresponding to an initial $^{26}Al/^{27}Al$ ratio of 1.2×10^{-5} in two anorthite-rich chondrules from Acfer 094.

To understand the genetic relationships between CAIs,

* Author to whom correspondence should be addressed (sasha@higp.hawaii.edu).

AOAs, and Al-rich chondrules (ARCs), we studied the mineralogy, petrography, bulk chemistry, Al-Mg and oxygen isotopic compositions of these objects in primitive carbonaceous chondrite groups and ungrouped meteorites, including CR (Aléon et al., 2002), CB (Krot et al., 2001a), Adelaide (Krot et al., 2001b,c; Huss et al., 2003) and Acfer 094 (Fagan et al., 2003) chondrites. Here we describe the mineralogy, petrology, and bulk chemistry of CAIs, AOAs and Al-rich (>10 wt% bulk Al_2O_3, Bischoff and Keil, 1984) chondrules from Acfer 094; Al-Mg and oxygen isotopic studies are in progress and will be reported elsewhere.

2. ANALYTICAL PROCEDURES

Three polished thin sections of Acfer 094 were mapped in Ca, Al, Mg, Ti, and Na Kα X-rays with resolutions of 7–10 μm per pixel with a Cameca SX50 electron microprobe. The elemental maps in Mg, Ca, and Al Kα were combined using a RGB-color scheme (Mg = red, Ca = green, Al = blue) and ENVI (environment for visualizing images) software. CAIs, AOAs and Al-rich chondrules identified in the combined X-ray maps were studied in the backscattered electron (BSE) mode with a JEOL 5900LV scanning electron microscope. Mineral compositions were determined with a Cameca SX50 electron microprobe using 15 kV accelerating voltage, with 10–20 nA beam current for silicates and 30 nA beam current for metal. Counting times on both peak and background were 10 s for Na and K and 3 s for all other elements. Minerals were measured with a focused (1–2 μm) beam. Glasses (mesostases and melt inclusions) were analyzed with a defocused beam (3–7 μm). Well-characterized silicates and oxides were used as standards. Matrix corrections were applied using a PAP software routine. Bulk compositions of CAIs, AOAs, and Al-rich chondrules were measured by acquiring ~15 × 15 μm rastered beam analyses along profiles covering a whole object. Detection limits in silicates were (in wt%) SiO_2, Al_2O_3, MgO 0.03; TiO_2, CaO, K_2O 0.04; Na_2O, Cr_2O_3 0.06; MnO 0.07; FeO 0.08.

3. RESULTS

3.1. Mineralogy and Petrology

Refractory inclusions and Al-rich chondrules are relatively common in Acfer 094 and comprise ~2 vol% of the rock (Fig. 1), consistent with the earlier observations by Weber et al. (1995).

3.1.1. Ca,Al-Rich inclusions and amoeboid olivine aggregates

Based on their mineralogy, refractory inclusions in Acfer 094 can be divided into corundum-rich, hibonite-rich, grossite-rich, spinel-melilite-rich (compact and fluffy Type A), and pyroxene-anorthite-rich CAIs, pyroxene-hibonite spherules, and AOAs (Table 1). Most of the CAIs are irregularly shaped objects that show no clear evidence for having ever been melted; few exceptions are two pyroxene-anorthite-rich CAIs with igneous textures, three pyroxene-anorthite-spinel fragments, a unique pyroxene-hibonite spherule, and a fragmented zoned melilite grain with spinel inclusions (compact Type A CAI). None of the CAIs contains secondary low-temperature minerals, such as nepheline, sodalite, grossular, wollastonite, hedenbergite, andradite, phyllosilicates, and magnetite which are commonly observed in the CV, CM, enstatite, and metamorphosed (petrologic types 3.1–3.9) CO chondrites (e.g., MacPherson et al., 1983, 1984, 1988; Lee and Greenwood, 1994; Russell et al., 1998; Fagan et al., 2000).

The *corundum-rich CAI* contains a corundum-hibonite core surrounded by a spinel mantle and a thin pyroxene rim; a small grain of anorthite occurs in its outer portion (Figs. 2a–d). The CAI core is highly porous; some of the porosity may have resulted from terrestrial weathering.

The *hibonite-rich CAI* consists of a hibonite-spinel-perovskite core surrounded by a melilite mantle (Fig. 2e). The CAI core contains abundant pores. Based on the pristine appearance of the CAI and the fact that the pores occupy regions between lath-shaped hibonite crystals, we conclude that this porosity is a primary signature of the inclusion. Two compositional types of hibonite were observed: Mg- and Ti-poor and Mg- and Ti-rich (Table AE1, an. 2, 3); it appears that the former is replaced by the latter. The only other hibonite-rich CAI is found inside a ferromagnesian porphyritic olivine (Type II) chondrule and is described in a separate section (see *CAI-bearing chondrule*).

Grossite-rich CAIs are rather common (~10% of all inclusions) (Table 1). They consist of grossite-perovskite ± spinel ± hibonite ± melilite cores surrounded by melilite or melilite-pyroxene rims and show large variations in modal mineralogy (Fig. 3). Perovskite is concentrated in grossite. Hibonite occurs as lath-shaped grains in spinel, and melilite forms rims around the cores. Secondary anorthite replacing melilite is very rare (Fig. 3d). One of the grossite-rich CAIs is anomalously enriched in perovskite and has a porous, hibonite-grossite-melilite-perovskite core surrounded by spinel + hibonite, melilite, and pyroxene layers (Figs. 3a,b).

Spinel-melilite-rich CAIs can be divided into two subtypes: (i) Irregularly shaped, porous inclusions texturally similar to the grossite-rich and hibonite-rich inclusions, but lacking grossite and hibonite. These inclusions consist of a spinel-perovskite ± melilite core surrounded by a melilite-pyroxene rim (Figs. 4a,b); secondary anorthite replacing melilite is very minor. (ii) Compact and fluffy Type A CAIs composed of melilite-spinel ± Al-diopside cores surrounded by pyroxene rims (Figs. 4c,d). Fluffy Type A CAIs, which are dominant, contain anhedral grains of spinel and Al-diopside embedded in melilite (Fig. 4d). Compact Type A CAI, which are very rare, contain euhedral spinel grains (Fig. 4c). Melilite in the outer portions of the CAIs is commonly replaced by anorthite.

Pyroxene-anorthite-rich CAIs consist of anhedral grains of Al-diopside, melilite heavily replaced by anorthite, and spinel, which appears to be corroded by anorthite as well (Figs. 4e,f). Al-diopside is largely concentrated in the outer portions of the CAIs, and in turn, may be surrounded by a rim of forsterite. There is a continuum in modal mineralogy between the melilite-rich and pyroxene-anorthite-rich CAIs (Figs. 4d–f), suggesting that the latter probably formed by replacement of the melilite-rich inclusions.

Two of the pyroxene-anorthite-rich CAIs can be classified as *Type C* inclusions: they have igneous textures and consist of euhedral and subhedral grains of Al-Ti-diopside and spinel

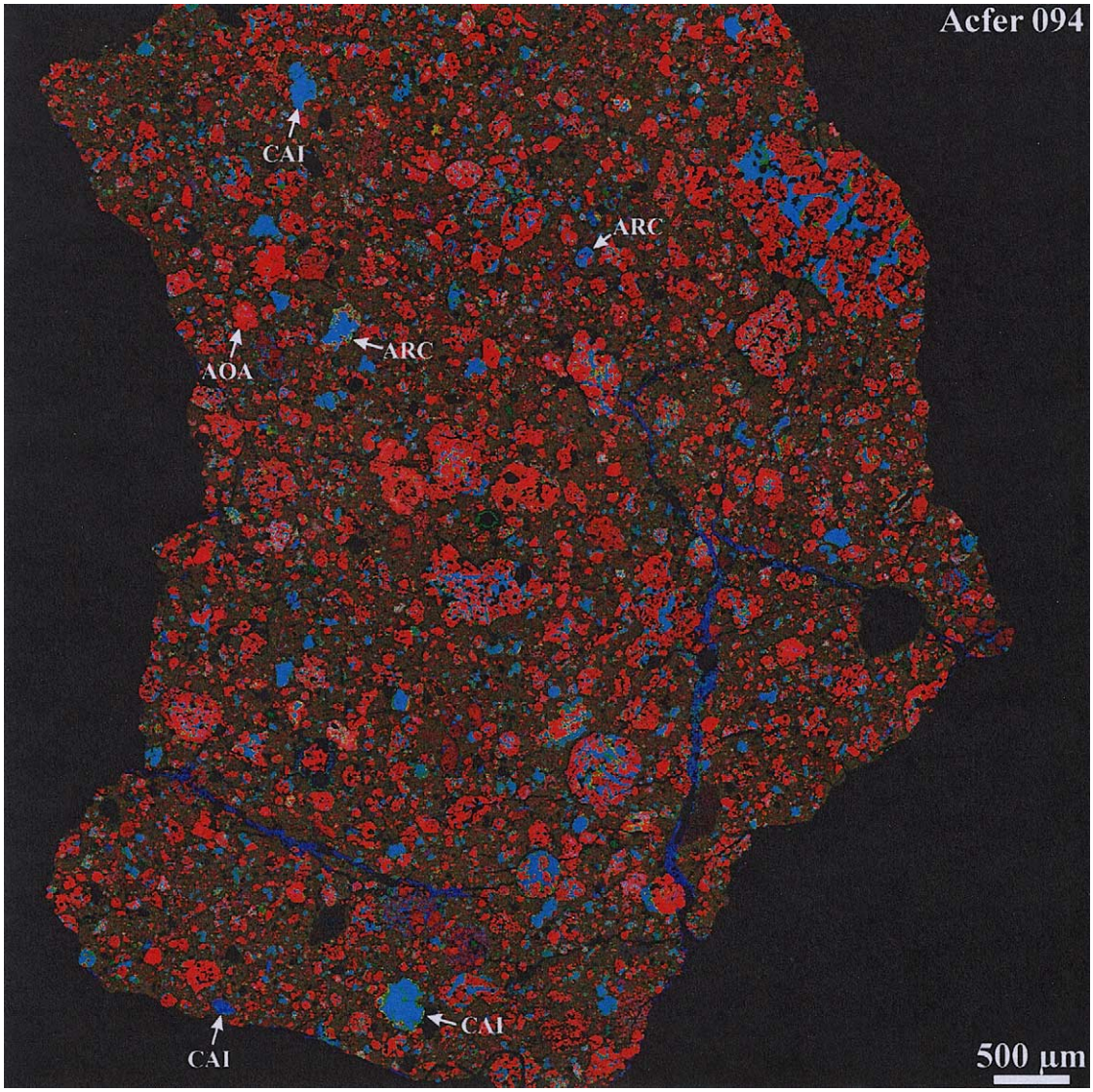

Fig. 1. Combined elemental map in Mg (red), Ca (green) and Al Kα (blue) X-rays of the unique carbonaceous chondrite Acfer 094. The meteorite contains ~2 vol% of Ca, Al-rich inclusions (CAIs), amoeboid olivine aggregates (AOAs) and Al-rich chondrules (ARCs).

surrounded by anorthite (Fig. 5). Both CAIs contain rare grains of low-Ca pyroxene and forsteritic olivine overgrown by Al-Ti-diopside and show no evidence for core-rim structure.

Amoeboid olivine aggregates consist of forsteritic olivine, FeNi-metal, and a refractory component composed of anorthite, Al-diopside, spinel, and very rare melilite (Fig. 6). There are large variations in both the modal mineralogy of the refractory component and refractory component/olivine ratios. Melilite is replaced by a symplectic intergrowth of spinel and Al-diopside (Fig. 6b). Spinel grains are typically anhedral and appear to be replaced by anorthite. Five out of ~100 AOAs studied by SEM and EPMA contain low-Ca pyroxene replacing olivine in the AOA peripheries (Figs. 6e,f). This is the first discovery of low-Ca pyroxene associated with refractory inclusions. AOAs with and without low-Ca pyroxene are texturally and mineralogically similar.

The *pyroxene-hibonite spherule* consists of an Al-rich pyroxene core with several lath-shaped crystals of hibonite, spinel and melilite (Fig. 7). Spinel is intergrown with hibonite and appears to replace it. Melilite occurs in the outer portions of the spherule and is extensively corroded by anorthite. The pyroxene core has very high and variable Al_2O_3 contents (23–44 wt%) and is surrounded by a thin rim of Al-diopside.

3.1.2. *Ca,Al-Rich inclusion-bearing chondrule*

Ferrous porphyritic olivine (Type II) chondrule 17 contains a relict hibonite-rich CAI (Fig. 8). The CAI consists of hibonite surrounded by a 5-μm-thick layer and numerous euhedral crystals of Fe-rich spinel embedded in chondrule mesostasis. Hibonite and spinel contain tiny inclusions of perovskite, Re-Ir-Os–bearing nuggets, and an unidentified Zr-bearing phase.

Table 1. Classification of refractory inclusions in Acfer 094.[a]

Type	Mineralogy	Number	%
Corundum rich	cor-hib-sp [cpx]	1	0.5
Pyroxene-hibonite-spherule	cpx-hib-sp-mel-an [cpx]	1	0.5
Hibonite rich	hib-pv-sp-mel [cpx]	2	1.1
Grossite rich	grs-pv ± mel ± hib ± sp [sp-mel-cpx ± an	16	8.5
Spinel-melilite rich	sp-pv ± mel ± hib ± an [cpx]	95	50.3
Pyroxene-anorthite rich	an-cpx-sp ± mel	14	7.4
Pyroxene-anorthite rich, type C	an-cpx-sp-ol-opx	3	1.6
AOAs	fo-met ± opx-cpx-an ± sp ± mel	57	30.2
Total		189	100

[a] An = anorthite; cor = corundum; cpx = A1, Ti-diopside; fo = forsterite; grs = grossite; hib = hibonite; mel = melilite; pv = perovskite; sp = spinel; met = FeNi-metal; ol = olivine; opx = low-Ca pyroxene.

The host chondrule consists of subhedral-to-euhedral ferrous olivines ($Fa_{33 \pm 5}$), interstitial anorthitic mesostasis (An_{70-93}), Fe-Cr-spinel, FeNi-sulfides, and rare forsteritic olivines (Fa_4) that are probably relict. Oxygen and Al-Mg isotopic studies of chondrule 17 have recently been reported by Krot et al. (1999). Here, we only summarize the results.

Hibonite is enriched in ^{16}O ($\delta^{18}O = -31$ to -36‰, $\delta^{17}O = -37$ to -42‰). Spinel is relatively ^{16}O-poor ($\delta^{18}O = -26$ to -32‰, $\delta^{17}O = -31$ to -32‰), probably due to overlap of the beam onto plagioclase mesostasis ($\delta^{18}O = -3$ to -6‰, $\delta^{17}O = -5$ to -8‰) in the adjacent chondrule. Within the chondrule, a relict forsterite grain is more ^{16}O-enriched ($\delta^{18}O = -5$‰, $\delta^{17}O = -7$‰) than the fayalitic olivines ($\delta^{18}O = +3$ to -3‰, $\delta^{17}O = +1$ to -5‰). Hibonite of the relict CAI is isotopically anomalous with $\delta^{26}Mg = -5 \pm 2$‰. Plagioclase of the host chondrule shows no resolvable $^{26}Mg^*$, implying an upper limit for $(^{26}Al/^{27}Al)_I$ of $<1 \times 10^{-5}$.

3.1.3. Al-Rich chondrules

Al-rich chondrules (ARCs) are relatively common in Acfer 094, but less abundant than refractory inclusions. Based on textures and mineralogy, ARCs can be divided into zoned (Figs. 9 and 10) and unzoned (Fig. 11) chondrules.

The zoned chondrules either have clear core-mantle structures (Figs. 9a–e) or contain mineralogically distinct portions (Figs. 9f, 10a–c). Cores of the chondrules s4 (Figs. 9a,b), 314 (Figs. 9c,d) and 335 (Fig. 9e) are FeNi-metal-free/poor and consist mainly of anorthitic plagioclase and high-Ca pyroxene; low-Ca pyroxene and forsteritic olivine are minor or absent. Mantle zones are FeNi-metal-rich and consist of low-Ca pyroxene, high-Ca pyroxene, forsteritic olivine and anorthitic plagioclase or mesostasis. Chondrule 3 (Fig. 9f) has two mineralogically distinct portions: one composed of anorthite and high-Ca pyroxene and another composed of low-Ca pyroxene, forsteritic olivine, and abundant FeNi-metal nodules.

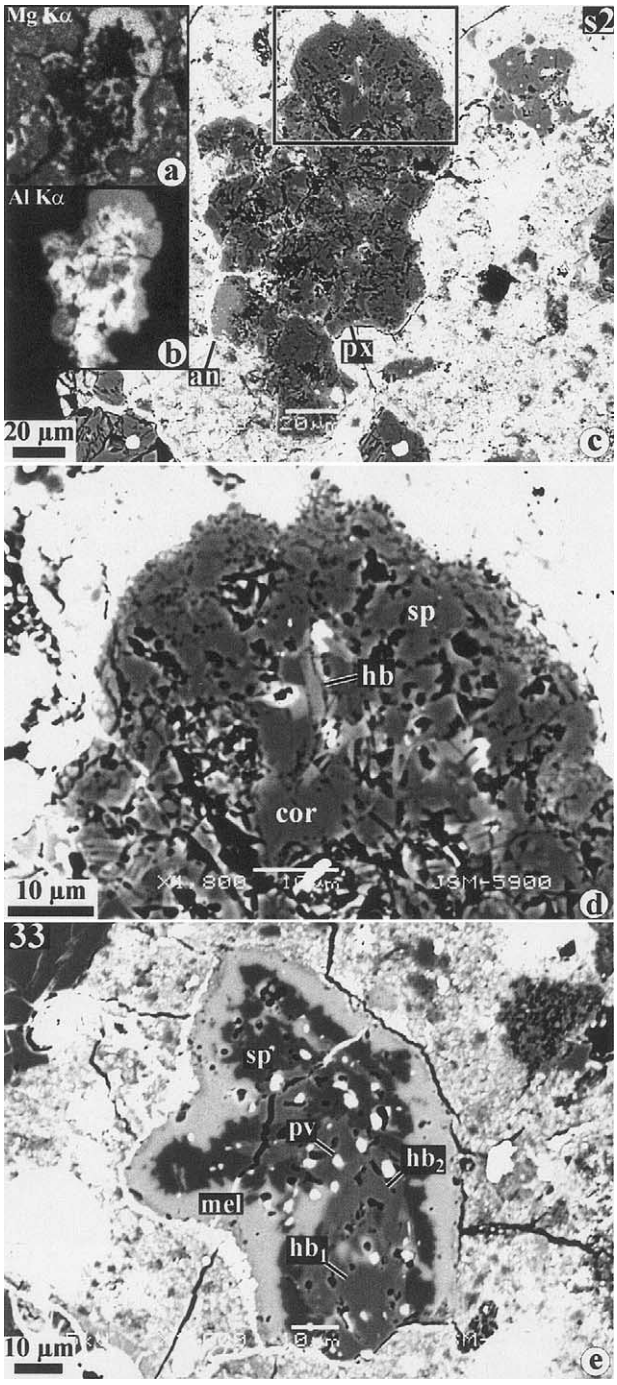

Fig. 2. Elemental maps in Mg (a) and Al Kα (b) X-rays and BSE images (c-e) of the corundum-rich CAI s2 (a-d) and hibonite-rich CAI 33 (e) from Acfer 094. The CAI s2 consists of a corundum-hibonite core surrounded by a spinel mantle and a thin pyroxene rim. Small grain of anorthite occurs in the outer portion of the inclusion. The CAI 33 is composed of a hibonite-spinel-perovskite core surrounded by a melilite rim. There are two compositional types of hibonite in the CAI: Ti-Mg-poor (hb_1) and Ti-Mg-rich (hb_2) (see Table AE1, an. 2, 3). Region outlined in (c) is shown in detail in "d." an = anorthite; cor = corundum; hb = hibonite; mel = melilite; px = Al-diopside; pv = perovskite; sp = spinel.

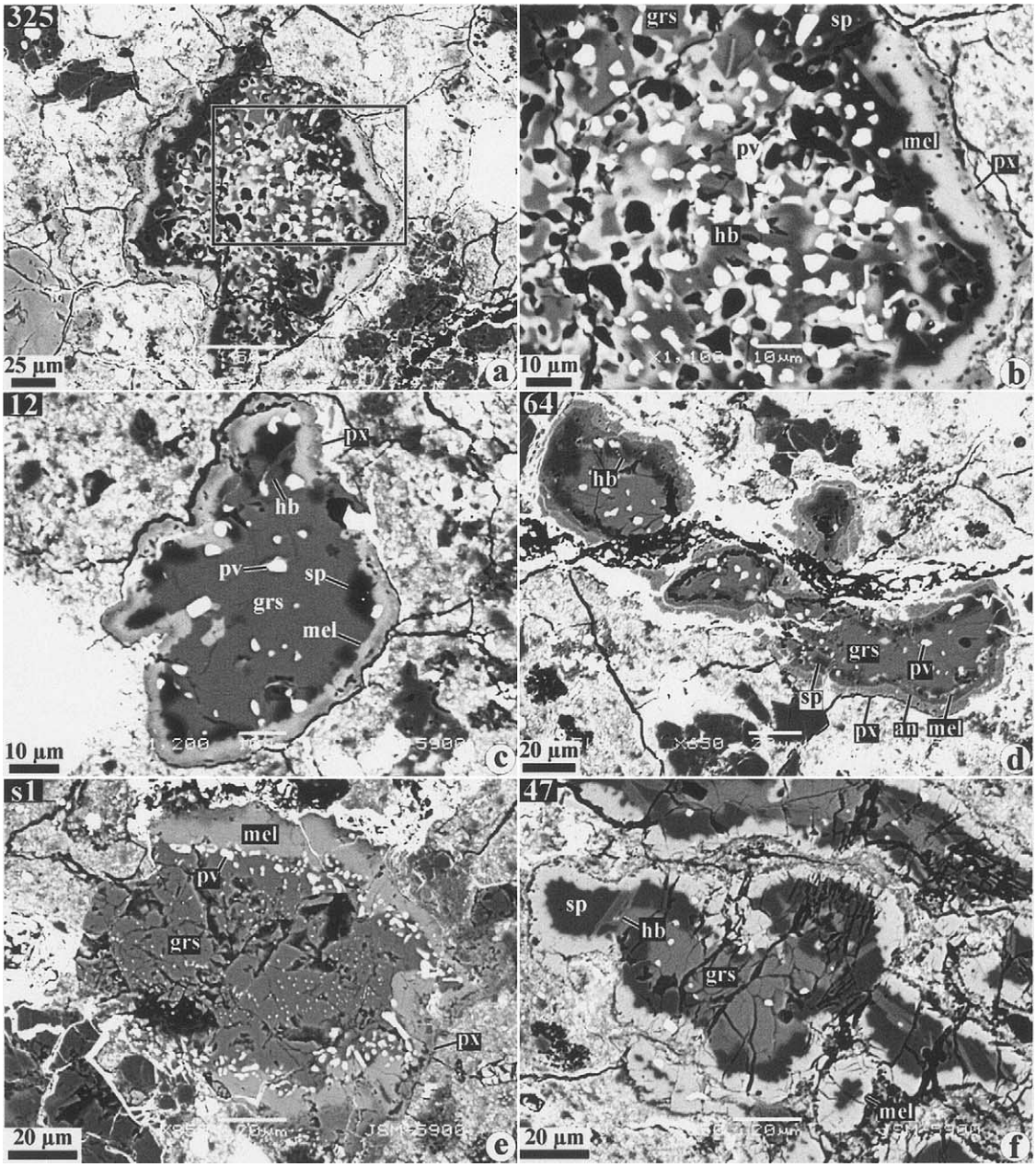

Fig. 3. BSE images of the grossite-rich CAIs from Acfer 094. The CAIs are irregularly shaped and have a grossite-perovskite ± spinel ± melilite ± hibonite core surrounded by a melilite rim or a melilite-Al-diopside rim. Melilite is occasionally replaced by anorthite. There are significant variations in modal mineralogy of the CAI cores. Region outlined in (a) is shown in detail in "b." grs = grossite.

Chondrules 300 (Figs. 10a,b), 215 (Fig. 10c), and 312 also contain mineralogically distinct portions; however, their Al-rich portions consist largely of anorthitic plagioclase and spinel, rather than anorthite and high-Ca pyroxene. The spinel grains are euhedral or subhedral, and occasionally contain inclusions of perovskite (identified by EDS); spinels either occur as clusters of grains surrounded by plagioclase (Fig. 10c) or individual grains enclosed by plagioclase or intergrown with low-Ca pyroxene (Fig. 10b). Ferromagnesian portions of the chondrules consist of forsteritic olivine, low-Ca pyroxene, FeNi-metal, high-Ca pyroxene, and glassy mesostasis; low-Ca pyroxene typically replaces olivine (Fig. 10c). Chondrule 313 (Fig. 10d) consists of low-Ca pyroxene phenocrysts replacing forsteritic olivine, coarse anorthite laths poikilitically enclosing spinel grains, FeNi-metal nodules, and crystalline mesostasis composed of anorthite and a silica phase.

The unzoned chondrules are rounded and mineralogically uniform (Fig. 11). They consist of elongated low-Ca pyroxene grains overgrown by high-Ca pyroxene and poikilitically enclosing olivine grains, FeNi-metal nodules, anorthitic plagio-

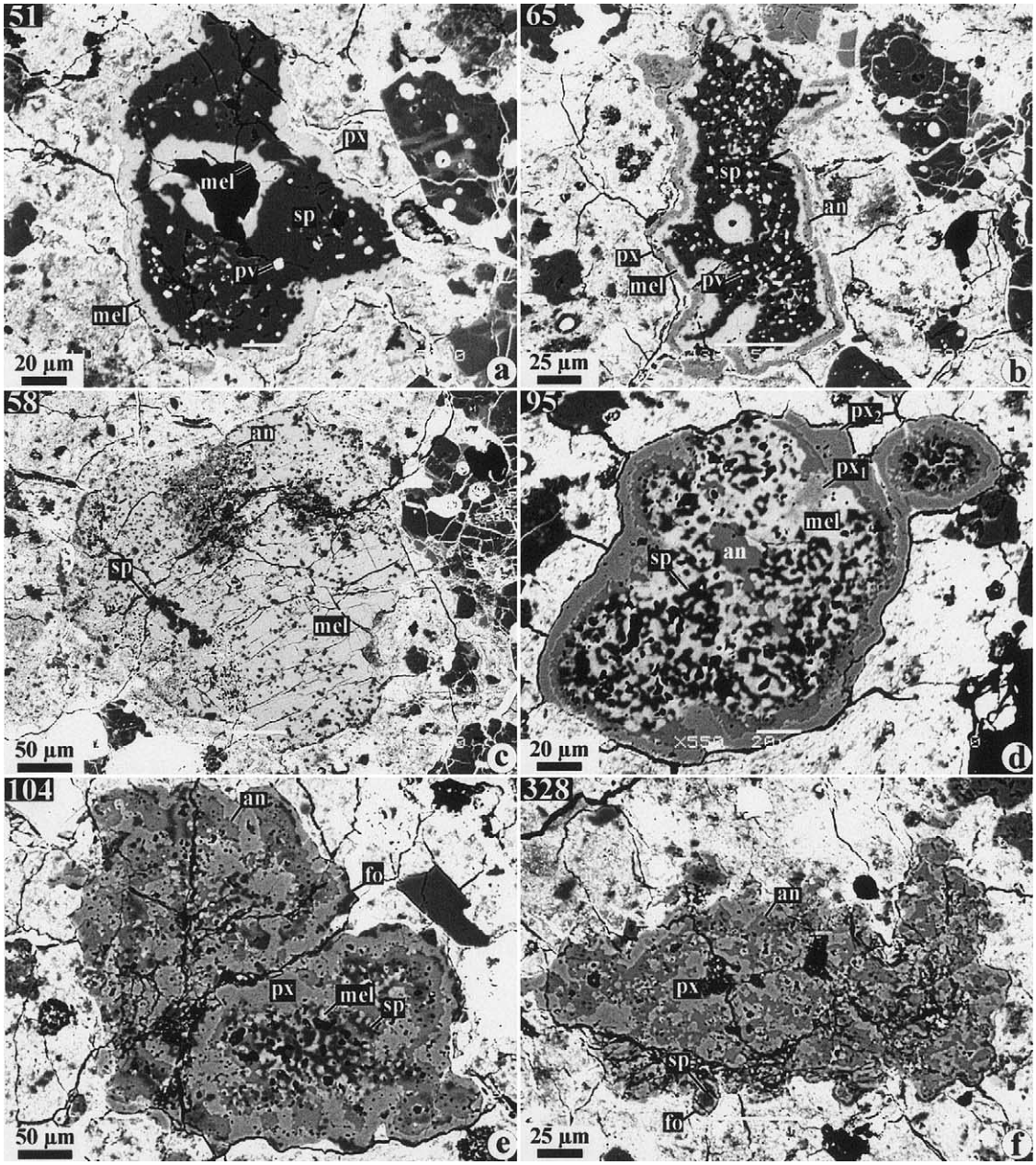

Fig. 4. BSE images of the spinel-rich (a, b), melilite-rich (c, d) and pyroxene-anorthite-rich (e, f) CAIs from Acfer 094. The spinel-rich CAIs (a, b) have spinel-perovskite-melilite cores surrounded by melilite ± anorthite-pyroxene rims; anorthite replaces melilite. The melilite-rich CAI 58 (c) consists of åkermanite-rich ($Åk_{62–69}$) melilite enclosing subhedral spinel grains; melilite is replaced by anorthite. The melilite-rich CAI 95 (d) has a more gehlenitic ($Åk_{18–26}$) melilite enclosing anhedral spinel grains and minor Al-Ti-diopside (px_1); melilite is replaced by anorthite and is surrounded by a rim of diopside (px_2). The pyroxene-anorthite-rich CAI 104 (e) has a spinel-melilite core extensively replaced by anorthite and surrounded by the rims of pyroxene and forsterite. The CAI 328 (f) has an anorthite core with minor spinel; the core is surrounded by a pyroxene-forsterite rim. fo = forsterite.

clase, and crystalline mesostasis composed of anorthite, high-Ca pyroxene, and a silica phase.

3.1.4. Pyroxene-Plagioclase-Spinel fragments with igneous textures

Three Ca-Al-rich fragments (Fig. 12) have igneous textures and are mineralogically distinct from the refractory inclusions and Al-rich chondrules described above. Fragment 11a consists of anorthitic plagioclase, Al-Ti-diopside, and forsterite (Fig. 12a). Fragment 8 consists of a large spinel grain overgrown by anorthitic plagioclase, and high-Ca pyroxene, and low-Ca pyroxene (Fig. 12b). Fragment 88 consists of coarse-grained Al-diopside, euhedral spinel grains, and minor anorthite (Fig. 12c).

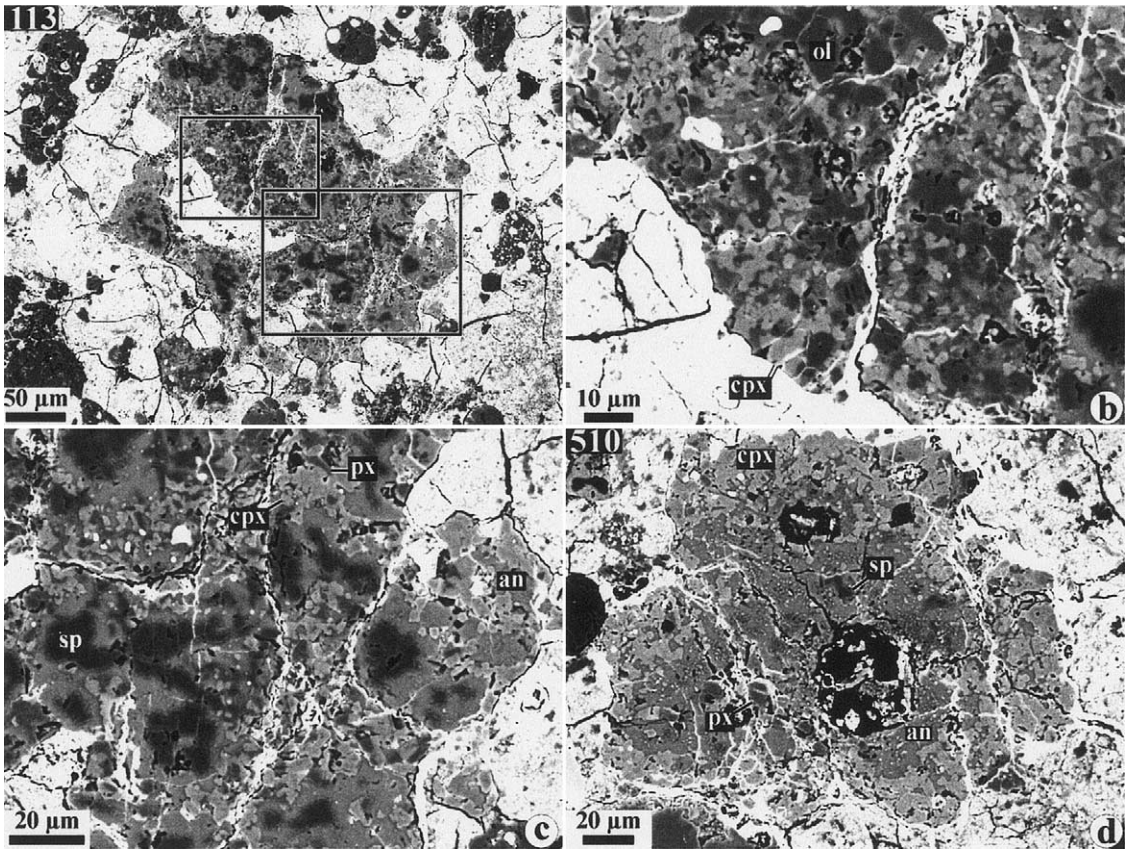

Fig. 5. BSE images of the pyroxene-anorthite-rich CAIs with igneous textures from Acfer 094. (a–c) CAI 113 consists of euhedral and subhedral grains of Al-Ti-diopside and spinel surrounded by anorthite. Low-Ca pyroxene and forsteritic olivine are rare minerals which are overgrown by Al-Ti-diopside. (d) CAI 510 consists of an anorthite-rich core with numerous inclusions of euhedral and subhedral grains of spinel and rare grains of low-Ca pyroxene; the core is surrounded by a layer of Al-diopside grains having euhedral shapes.

3.2. Mineral Chemistry

Corundum is nearly pure Al_2O_3, and *grossite* is nearly pure $CaAl_4O_7$ (Table AE1).[1] *Hibonite* shows large variations in TiO_2 and MgO (Table AE1; Fig. 13). Two of the hibonite-rich inclusions contain low-Ti, low-Mg hibonite coexisting with high-Ti, high-Mg hibonite (Table AE1, an. 2–5); it appears that the former is replaced by the latter (Fig. 2e). Relict hibonite in chondrule 17 (Fig. 8) is characterized by low TiO_2 and MgO contents (Table AE6).

Melilite is Na-free and ranges from $Åk_1$ to $Åk_{70}$; most analyses are in the range of $Åk_{1–20}$ (Table AE2; Fig. 14). The highest åkermanite content was found in compact Type A CAI 58 containing euhedral inclusions of spinel (Fig. 4c). Compositional variations of melilite within an individual CAI are small (<10 mol% Åk); melilites from the grossite- and hibonite-rich CAIs tend to have lower Åk contents than those from the less refractory, spinel-melilite-rich CAIs (Fig. 14).

Plagioclase in most CAIs and AOAs is nearly pure $CaAl_2Si_2O_8$; the only exception is plagioclase from Type C CAI 113 (Figs. 5a–c), which contains 0.18 wt% Na_2O (Table AE3). Plagioclase grains in both zoned and unzoned Al-rich chondrules contain 0.1–0.4 wt% Na_2O (Table AE3). The highest Na_2O contents (0.74–3.4 wt%) were found in plagioclase grains in Type II chondrule 17 with relict CAI (Fig. 8).

High-Ca pyroxenes in CAIs and AOAs are typically characterized by very low (or below detection limits) MnO and Cr_2O_3 contents (Table AE4; Fig. 15); Al_2O_3 and TiO_2 range from 0 to 45 wt% and 0–4.5 wt%, respectively. The Al contents in diopside generally increase towards spinel or anorthite grains. The highest Al_2O_3 contents were found in the pyroxene-hibonite spherule 86 (Fig. 7). Compared to the high-Ca pyroxenes in refractory inclusions, those in ARCs have higher MnO and Cr_2O_3 and similar TiO_2 and Al_2O_3 contents (Table AE4; Fig. 15). High-Ca pyroxenes in igneous-textured pyroxene-plagioclase-spinel fragments are characterized by high Al_2O_3 and relatively high TiO_2 and Cr_2O_3 contents (Table AE4; Fig. 15).

Low-Ca pyroxenes ($Wo_{0.7–2.7}$) in AOAs are magnesium-rich ($Fs_{0.6–1}$) and characterized by low TiO_2 (0.03–0.27 wt%), Al_2O_3 (0.21–0.54 wt%), Cr_2O_3 (0.28–0.33 wt%), and MnO (0.08–0.12 wt%) (Table AE5). Poor stoichiometry and high FeO of some of the analyses are due to the presence of terrestrial weathering products, small grain sizes of low-Ca pyroxenes, and their close

[1] Tables AE1-AE6 are in an electronic annex (Elsevier website, ScienceDirect).

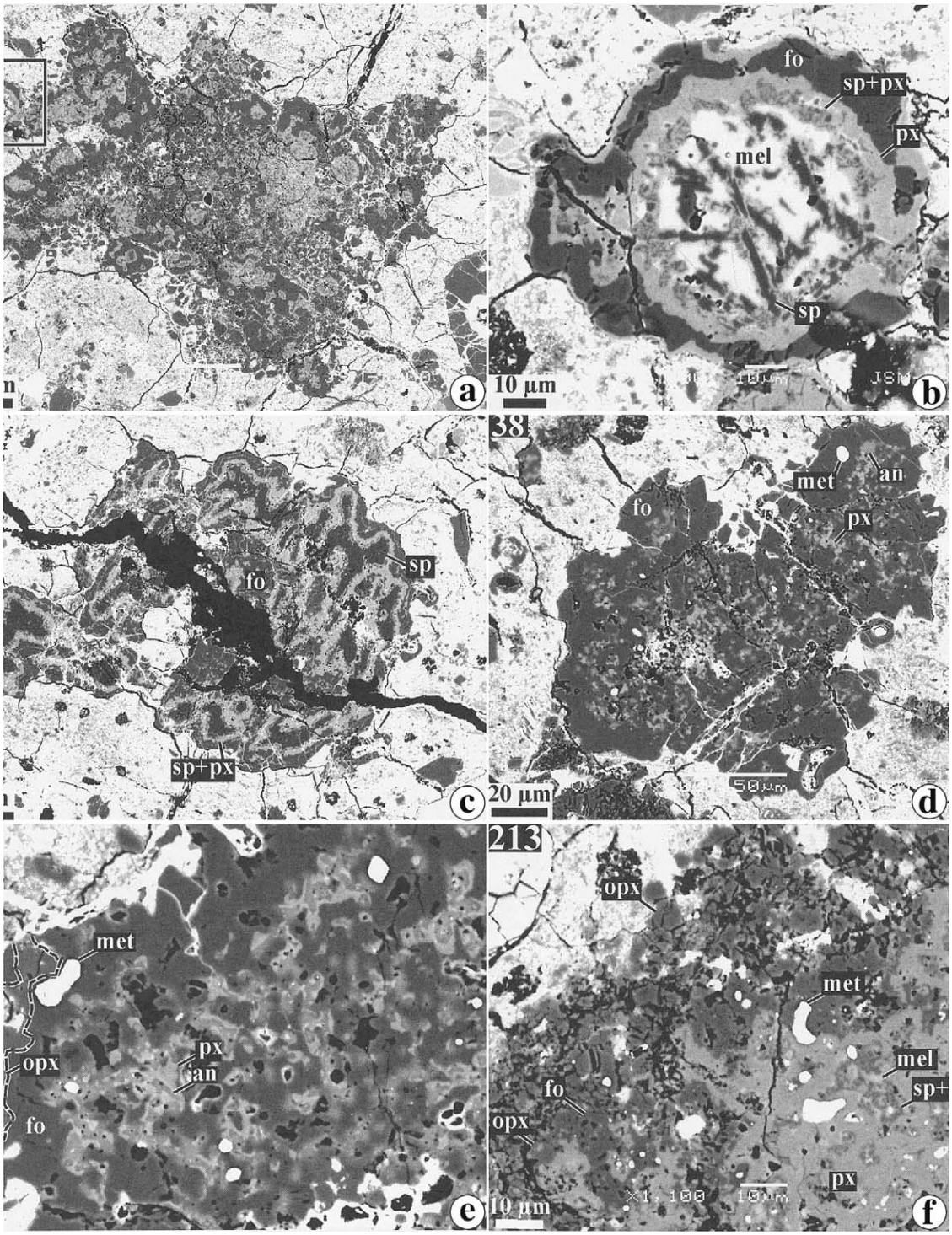

Fig. 6. BSE images of AOAs from Acfer 094. The AOAs consist of forsteritic olivine, FeNi-metal, and a refractory component composed of anorthite, Al-diopside, ± melilite, ± spinel. Melilite is replaced by symplectitic intergrowths of spinel and Al-diopside. There are large variations in the modal mineralogy of the refractory component and refractory component/olivine ratios. Forsterite grains in outer portions of the AOAs 105 (e) and 213 (f) are replaced by low-Ca pyroxene. Region outlined in (a) is shown in detail in "b." met = FeNi-metal; px = low-Ca pyroxene.

intergrowths with forsteritic olivine. Low-Ca pyroxenes and pigeonites in ARCs contain systematically higher TiO_2 (0.15–1.8 wt%), Al_2O_3 (0.91–8 wt%), and Cr_2O_3 (0.56–1.1 wt%), compared to those in AOAs (Table AE5).

Spinel grains in CAIs, AOAs, and ARCs are magnesium-rich (except in relict CAI 17) and have low TiO_2 and Cr_2O_3 (<1.7 wt%). Spinels in chondrule 17 (Fig. 8) are iron-rich (Table AE6).

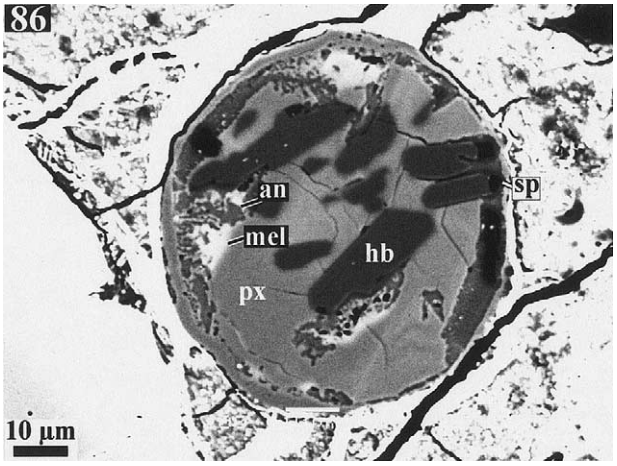

Fig. 7. BSE image of a pyroxene-hibonite spherule from Acfer 094. The spherule consists of high-Ca pyroxene, hibonite, spinel, and melilite partly replaced by anorthite. The pyroxene core has very high and highly variable Al_2O_3 contents. It is surrounded by a rim of Al-diopside.

Olivine grains in AOAs and rims around CAIs are nearly pure forsterite ($Fa_{<2}$) and typically have low Cr_2O_3 and MnO contents (Fig. 16). Olivine grains in the outer portions of some of the AOAs are enriched in MnO (up to 1.7 wt%) compared to those in their cores (~0.5 wt%). Olivine grains in AOAs with and without low-Ca pyroxene are compositionally similar. Olivine grains in ARCs are magnesium-rich ($Fa_{<2}$) and slightly enriched in Cr_2O_3 (0.3–0.7 wt%) compared those in AOAs and CAIs (Fig. 16).

3.3. Bulk Chemistry

Bulk compositions of CAIs, AOAs and ARCs from Acfer, together with the trajectory representing the bulk composition of solids condensed at equilibrium from a cooling gas of solar composition, are plotted on a phase diagram representing a projection from spinel onto the plane larnite-forsterite-corundum (Fig. 17). The bulk compositions of CAIs, ordered according to volatility (hibonite-rich, grossite-rich → spinel-melilite-rich → pyroxene-anorthite-rich) generally follow the condensation trajectory, but are systematically enriched in Al_2O_3. Bulk compositions of AOAs occupy a region between Al-diopside, anorthite, and forsterite, reflecting their mineralogy (Fig. 6) and origin as aggregates of forsterite and a refractory component composed of anorthite, Al-diopside and spinel (Grossman and Steele, 1976; Komatsu et al., 2000). All AOAs (except one) plot to the left of the anorthite-forsterite thermal divide. Bulk compositions of ARCs plot near the field occupied by pyroxene-anorthite-rich CAIs and AOAs, but to the right of the thermal divide (Fig. 17).

4. DISCUSSION

4.1. Pristine Nature of Ca,Al-Rich Inclusions, Amoeboid Olivine Aggregates and Al-Rich Chondrules in Acfer 094

The pristine nature of Acfer 094 has previously been inferred from its matrix mineralogy, dominated by amorphous material and submicron-sized forsterite and low-Ca pyroxene (Greshake, 1997), and from the very high abundances of presolar SiC and diamonds (Gao et al., 1996; Newton et al., 1995). The CAIs, AOAs, and ARCs studied here show no evidence for secondary alteration that resulted in formation of the secondary nepheline, sodalite, grossular, wollastonite, hedenbergite, andradite, ferrous olivine, carbonates, phyllosilicates, and magnetite in CAIs, AOAs, and chondrules in enstatite and CM, CO and CV carbonaceous chondrites (e.g., MacPherson et al., 1988; Jones and Brearley, 1994; Russell et al., 1998; Fagan et al., 2000; Komatsu et al., 2000). Based on these observations, we infer (i) Acfer 094 is a mineralogically pristine rock that escaped thermal metamorphism and aqueous alteration, (ii) the observed reaction relationships between minerals in CAIs and AOAs in Acfer 094 must have occurred in a nebular setting, and (iii) Acfer 094 is a very important meteorite for understanding both the physicochemical conditions during the formation of refractory inclusions and chondrules, and the original distribution of short-lived radionuclides and oxygen isotopes in these components (e.g., Fagan et al., 2003).

We note that neither refractory inclusions nor Al-rich chondrules in primitive meteorites such as CR (Weber and Bischoff, 1997; Aléon et al., 2002; Krot and Keil, 2002), CH (Krot et al., 2002c; McKeegan et al., 2003), CB (Krot et al., 2001a,b), and Acfer 094 (this study) show evidence for Fe-alkali metasomatic alteration, whereas both refractory inclusions and Al-rich chondrules in less primitive CV (e.g., MacPherson et al., 1988; Kimura and Ikeda, 1997; Krot et al., 2002b) and metamorphosed CO chondrites (e.g., Kurat and Kracher, 1980; Jones and Brearley, 1994; Hutcheon and Jones, 1995; Jones and Hutcheon, 1996; Russell et al., 1998) contain secondary Fe- and alkali-rich secondary phases. These observations suggest that the Fe-alkali metasomatic alteration of the CO and CV refractory inclusions and chondrules most likely occurred in the same location, nebular or asteroidal. Based on the differences in bulk chemistry and isotope chemistry (oxygen and magnesium) between CAIs and Al-rich chondrules, and the presence of ^{16}O-rich forsterite-rich accretionary rims around igneous, Type B CAIs in CV chondrites, Krot et al. (2002c) concluded that CAIs had been largely absent from the chondrule-forming region(s) at the time of chondrule formation. If this is the case, the correlated presence or absence of altered CAIs and chondrules in carbonaceous chondrites may imply that this alteration occurred in an asteroidal setting (Krot et al., 1995, 1998). This conclusion is consistent with the observed correlation between the degree of the alteration and metamorphic type of the CO chondrites (e.g., Russell et al., 1998).

4.2. Ca,Al-Rich Inclusions: I. Evidence for a Condensation Origin, Gas-Solid Nebular Reactions, Isolation, and Remelting

The mineralogy, petrology, textures, and bulk chemical compositions of CAIs from Acfer 094 suggest that most of them represent gas-solid nebular condensates, rather than evaporative residues or remelted condensates. This conclusion is supported by the following observations: (i) Most CAIs in Acfer 094 are irregularly shaped, porous objects; CAIs with igneous textures and subhedral-to-euhedral spinel and pyroxene grains are very rare. (ii) Many CAIs are mineralogically zoned, with the peripheries being less refractory than the cores, suggesting the CAIs are not evaporative residues. (iii) Melilite in CAIs is

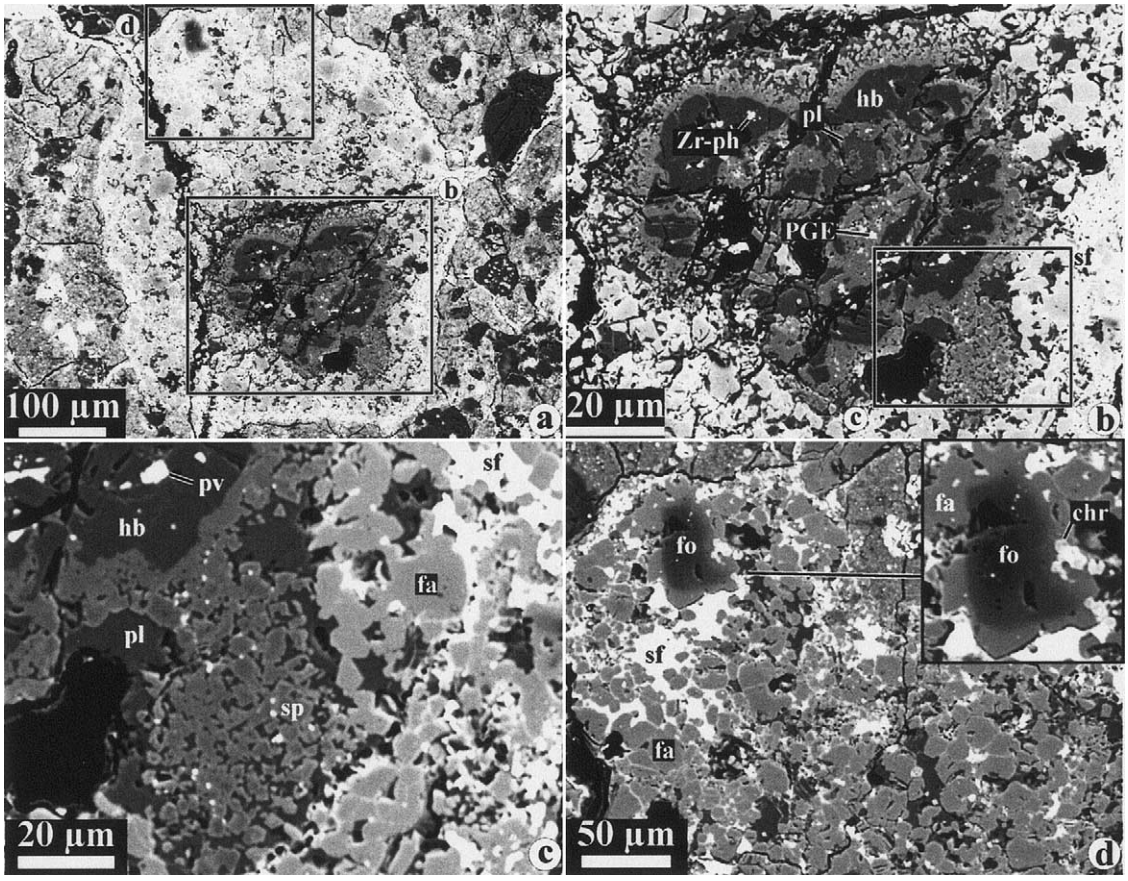

Fig. 8. BSE images of the CAI-bearing chondrule 17 from Acfer 094. The relict CAI consists of hibonite with inclusions of perovskite, a Zr-bearing phase (Zr-ph), and Re, Ir, Os-bearing (PGE) nuggets. It is surrounded by a shell of fine-grained, Fe-rich spinel (sp). The host chondrule consists of ferrous olivine (fa), plagioclase mesostasis (pl), FeNi-sulfides (sf), Fe-Cr-spinel (chr), and relict grains of forsteritic olivine (fo). Regions outlined in (a) are shown in detail in (b) and (d); region outlined in (b) is shown in detail in "c."

commonly replaced by a fine-grained mixture of spinel and diopside, and/or by anorthite and diopside.

The mineralogical zoning of the CAIs and the mineralogy of alteration products of melilite are generally consistent with the predicted condensation sequence of a gas of solar composition with the exception of spinel formation before melilite, a common feature of CAIs that has yet to be satisfactorily explained (e.g., Yoneda and Grossman, 1995; Petaev and Wood, 1998; Ebel and Grossman, 2000).

The gas-solid reactions responsible for the nebular alteration of melilite are predicted to occur in a cooling gas of solar composition (MacPherson et al., 2002; Krot et al., 2004), e.g.,

$$Ca_2Al_2SiO_7 + 3\,SiO(g) + 3\,Mg(g) + 6\,H_2O(g) = 2\,CaMgSi_2O_6 + MgAl_2O_4 + 6\,H_2(g) \quad (1)$$

$$Ca_2Al_2SiO_7 + 3\,SiO(g) + Mg(g) + 4\,H_2O(g) = CaAl_2Si_2O_8 + CaMgSi_2O_6 + 4\,H_2(g) \quad (2)$$

The observed increase of the Al contents in high-Ca pyroxenes towards spinel grains in CAIs containing little or no melilite may have resulted from reaction of spinel with diopside (reaction 3) or from replacement of melilite (reaction 4):

$$MgAl_2O_4 + CaMgSi_2O_6 + 0.5\,SiO(g) + 0.5\,H_2O(g) = 0.5\,CaAl_2Si_2O_8 + Mg_2SiO_4 + 0.5\,CaAl_2SiO_6 + 0.5\,H_2(g) \quad (3)$$

$$Ca_2Al_2SiO_7 + 2\,SiO(g) + Mg(g) + 3\,H_2O(g) = CaAl_2SiO_6 + CaMgSi_2O_6 + 3\,H_2(g)\,. \quad (4)$$

Although most of the grossite- and hibonite-rich CAIs are melilite-bearing and appear to be gas-solid condensates, only a few show evidence for gas-solid interactions leading to formation of anorthite (Fig. 3d). These observations and the presence of CAIs of different volatility in Acfer 094 suggest that these CAIs experienced different degrees of interaction with the cooling nebular gas. This may imply that the CAIs of different volatility were isolated from the nebular gas at different ambient nebular temperatures (Krot et al., 2002c).

The unambiguous condensation origin and pristine nature of the CAIs from Acfer 094 provides a unique opportunity for studying problems of nebular condensation that are still not well-understood. The famous spinel-melilite condensation discrepancy mentioned above is one of them. Condensation of spinel before melilite can be explained either by a kinetic delay

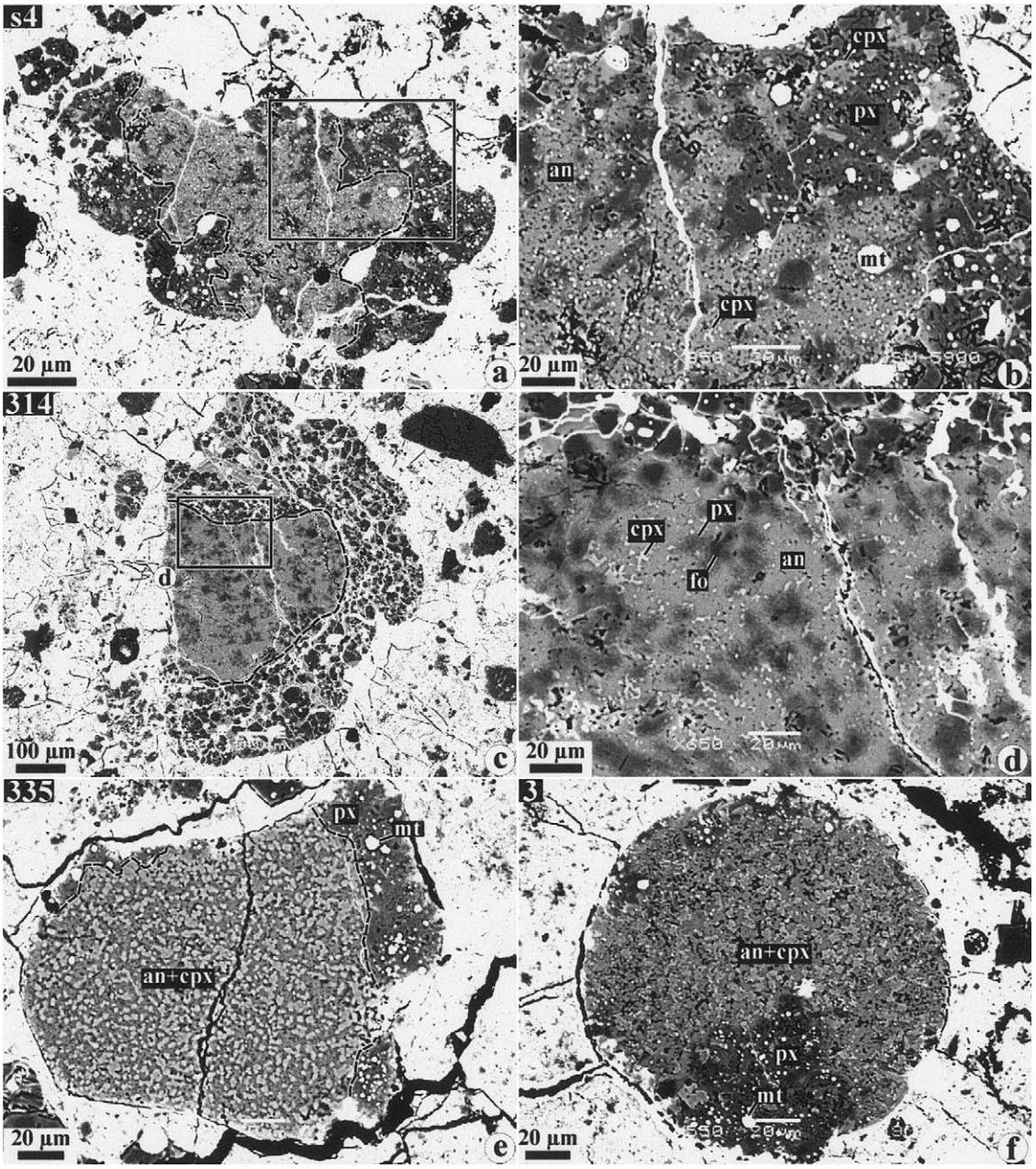

Fig. 9. BSE images of the Al-rich chondrules composed of the mineralogically distinct portions from Acfer 094. Chondrule s4 (a, b) has an anorthite-rich core (outlined in (a)) surrounded by a low-Ca pyroxene mantle containing abundant FeNi-metal (mt) nodules. Chondrule 314 (c, d) has an anorthite-rich core (outlined in (c)) which is FeNi-metal-free and contains tiny grains of high-Ca pyroxene and anhedral low-Ca pyroxene grains poikilitically enclosing forsteritic olivine. The core is surrounded by an olivine-pyroxene mantle having a porphyritic texture and containing abundant FeNi-metal nodules. Chondrule fragment 335 (e) consists of an anorthite-high-Ca pyroxene zone (outlined) which is FeNi-metal-free and an FeNi-metal-rich zone composed of low-Ca pyroxene. Chondrule 3 (f) has two mineralogically distinct portions: the dominant portion is composed of anorthite and high-Ca pyroxene (cpx); the minor portion consists of low-Ca pyroxene, forsteritic olivine, and abundant FeNi-metal nodules. Regions outlined in (a) and (c) are shown in detail in (b) and (d), respectively.

of the melilite condensation by ~100 K (Beckett and Stolper, 1994) or by condensation of melilite-free cores from fractionated nebular systems of nonsolar composition. Neither alternative has been explicitly explored so far.

Here we used the CWPI (*C*ondensation *W*ith *P*artial *I*solation) code (Petaev et al., 2003) to test these alternatives. The calculations were done at nebular pressure of 10^{-4} bar. The delay of melilite condensation modeled by the removal of gehlenite and åkermanite from the thermodynamic database results in the increase of the stability field of grossite and the appearance of $CaAl_2O_4$, larnite, rankinite, and wollastonite in the condensation sequence of the gas of solar composition.

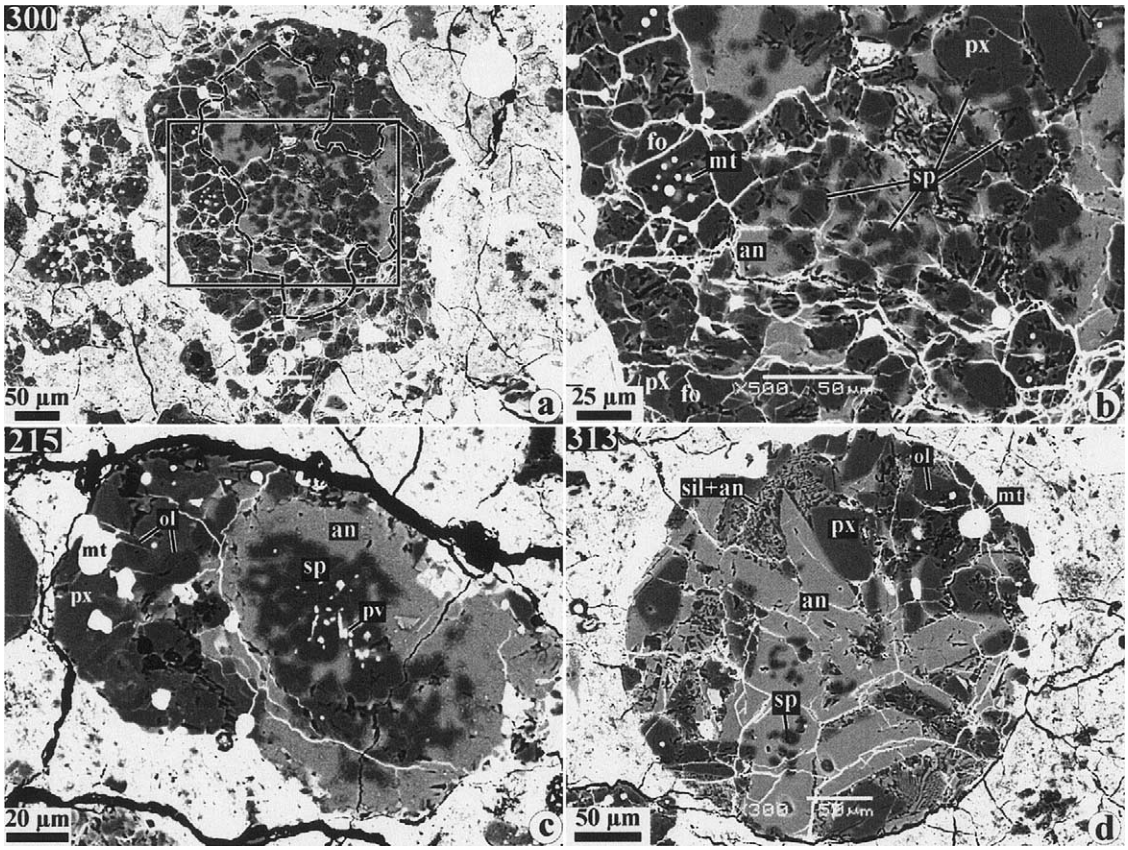

Fig. 10. BSE images of the Al-rich chondrules containing spinel-rich regions (remelted CAIs?) from Acfer 094. Chondrule 300 (a, b) has a spinel-anorthite-rich core (outlined in (a)) surrounded by an olivine-low-Ca pyroxene zone; olivine is replaced by low-Ca pyroxene. Chondrule fragment 215 (c) contains a cluster of spinel grains containing tiny inclusions of perovskite and surrounded by an anorthite layer; another portion of the chondrule contains FeNi-metal nodules and forsteritic olivine replaced by low-Ca pyroxene. Chondrule 313 (d) consists of low-Ca pyroxene phenocrysts corroding forsteritic olivine, anorthite laths poikilitically enclosing spinel grains, FeNi-metal nodules, and crystalline mesostasis composed of anorthite and a silica (sil) phase. Region outlined in (a) is shown in detail in (b).

Moreover, there is no spinel in such a condensation sequence. This along with the lack of Si in the cores of the hibonite- and grossite-rich inclusions hints that these CAIs condensed out of fractionated systems. An obvious assumption on condensation of these inclusions from Si-depleted nebular systems does not work. Although the condensation temperature of melilite is suppressed and a number of Ca-rich phases condensed before it, spinel still condenses after melilite regardless of the degree of Si depletion. Nebular systems enriched in Al or Mg also do not condense spinel before melilite. Only in the systems depleted in Ca by 84.4% or more, spinel condenses before melilite, with the temperature gap between these two minerals widening as the Ca depletion increases. For example, the equilibrium condensation sequence of the system depleted in Ca by 85% with the solar abundances of other elements is as follows: corundum (1705–1419 K), hibonite (1595–1415 K), Ti_3O_5 (1582–1545 K), perovskite (1545–1394 K), spinel solid solution (1420–1321 K), Mg-poor melilite solid solution (1416–1390 K), Al,Ti-rich clinopyroxene (1399–1322 K), anorthite (1321 K), forsterite (1381 K), etc. The depletion of the system in Ca delays condensation of all Ca-bearing minerals compared to the system of solar composition. Another consequence of the Ca depletion is the appearance of Ti_3O_5 in the condensation sequence that can be viewed as the evidence for condensation of Ti in hibonite if appropriate thermodynamic data would be included in the database. Making a simplistic assumption that both hibonite and Ti_3O_5 condense into a single phase, one can calculate Ti content of $\sim$ 0.2 wt% in late hibonite. This example demonstrates that condensation of a Ca-depleted system can account for the mineralogies and textures of hibonite- and spinel-rich inclusions, but not the grossite-rich ones. Obviously, grossite and spinel compete for Al, so the Ca/Mg ratio of a condensing system determines what mineral prevails. It is possible, that further adjustment of elemental abundances in fractionated nebular system may result in even better matches between the observed and calculated mineralogical and chemical compositions of CAIs, but it is beyond the scope of this work. The question 'Where and how such fractionated systems may be created?' still remains to be answered.

A few CAIs in Acfer 094 appear to have been melted. These include type C CAIs 113 and 510 (Fig. 5), a hibonite-pyroxene spherule 86 (Fig. 7), and a compact Type A CAI 58 (Fig. 4c) with euhedral spinel grains and åkermanite-rich melilite. Other

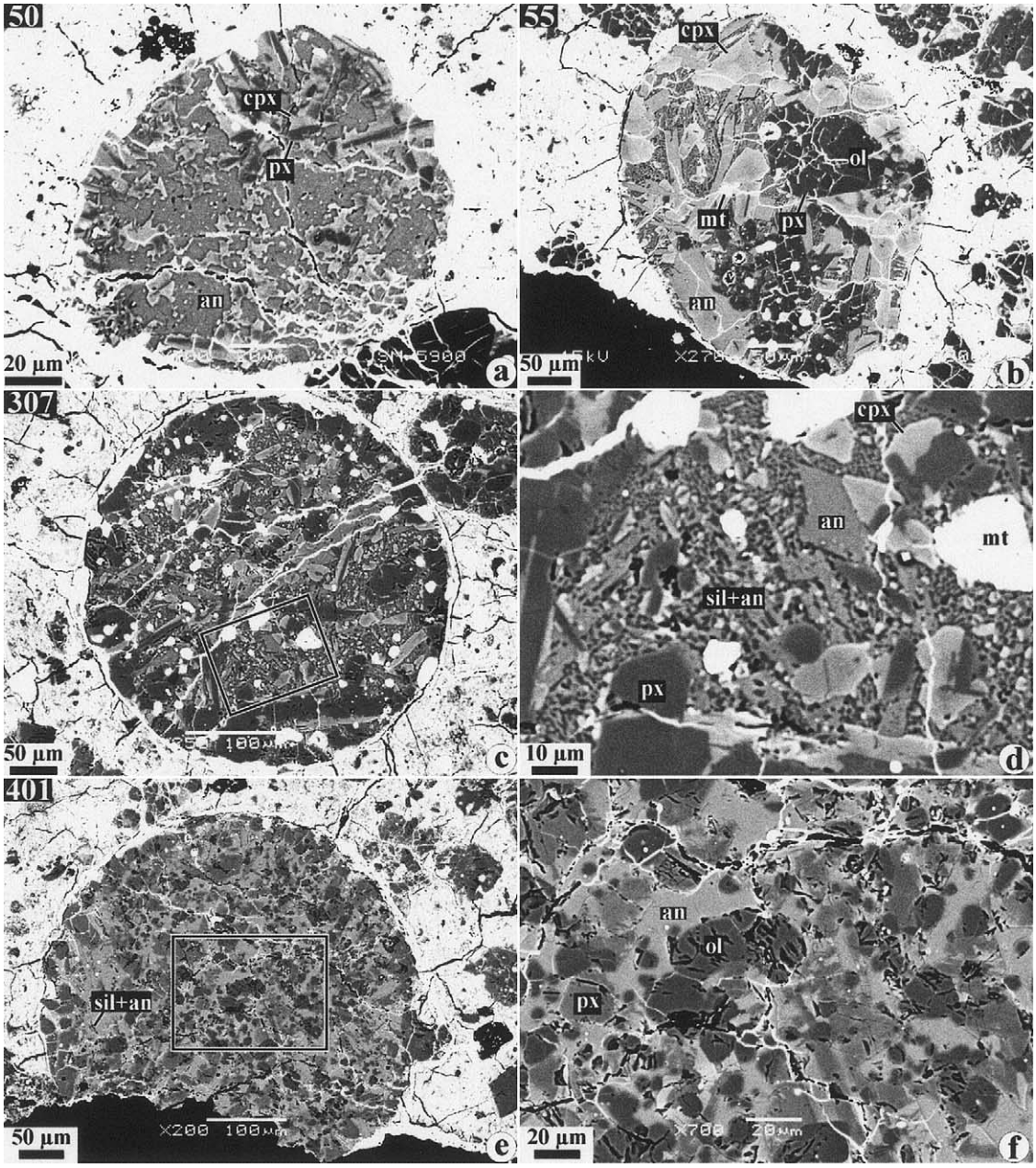

Fig. 11. BSE images of the extensively melted Al-rich chondrules from Acfer 094. These chondrules are rounded and contain no relict grains or mineralogically distinct regions. Chondrule 50 (a) consists of elongated low-Ca pyroxene grains overgrown by high-Ca pyroxene and surrounded by anorthite. Chondrule 55 (b) consists of low-Ca pyroxene phenocrysts poikilitically enclosing forsteritic olivine and FeNi-metal nodules, coarse-grained high-Ca pyroxene, lath-shaped anorthitic plagioclase, and crystalline mesostasis composed of anorthitic plagioclase, high-Ca pyroxene, and a silica phase. Chondrule 307 (c, d) consists of low-Ca pyroxene phenocrysts and elongated grains overgrown by high-Ca pyroxene, FeNi-metal nodules, and crystalline mesostasis composed of anorthitic plagioclase, high-Ca pyroxene, and a silica phase. Chondrule 401 (e, f) consists of low-Ca pyroxene, forsteritic olivine, anorthite, and crystalline mesostasis composed of anorthitic plagioclase, high-Ca pyroxene, and a silica phase. Regions outlined in (c) and (e) are shown in detail in (d) and (f), respectively.

igneous objects possibly related to CAIs are pyroxene-plagioclase fragments with igneous textures (Fig. 12).

4.3. Ca,Al-Rich Inclusions: II. Comparison with CAIs from Other Chondrite Groups

The first comparison of CAIs from Acfer 094 with those from other chondrite groups was made by Weber et al. (1995). Based on their study of 23 CAIs from Acfer 094, they concluded that these CAIs are mineralogically distinct from those in CV, CM, and CH chondrites, and are similar to those from CO and CR chondrites. Our study of ~ 200 refractory inclusions in Acfer 094 provides a more complete comparison. There are primary mineralogical differences between CAIs from Acfer 094 and those from CV, CM, CH, CB and CR chondrites.

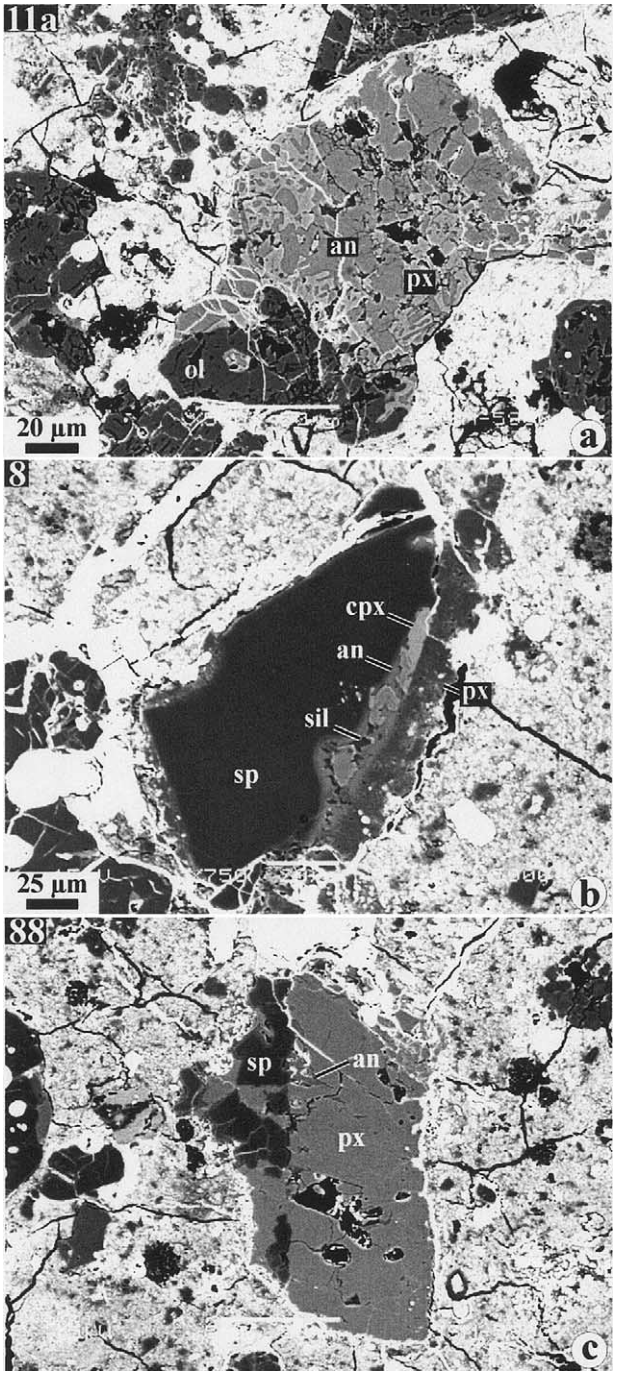

Fig. 12. BSE images of the refractory fragments having igneous textures from Acfer 094. Fragment 11a (a) consists of anorthitic plagioclase, Al-Ti-diopside, and forsterite. Fragment 8 (b) consists of a large spinel grain overgrown by anorthitic plagioclase, and high-Ca pyroxene, and low-Ca pyroxene. Fragment 88 (c) consists of coarse-grained Al-diopside, euhedral spinel grains, and minor anorthite.

CAIs in CV chondrites are significantly larger and less refractory on average than those in Acfer 094: grossite- and hibonite-rich CAIs are very rare in CV chondrites (e.g., MacPherson et al., 1988). It appears that most CV CAIs experienced complex formation histories involving multiple heating and possibly melting episodes (e.g., MacPherson and Davis, 1993; Yurimoto et al., 1994, 1998; Connolly and Burnett, 1999; Hsu et al., 2000; MacPherson et al., 2002). In addition, some CAI types are found only in CV chondrites, e.g., Type B and forsterite-bearing CAIs.

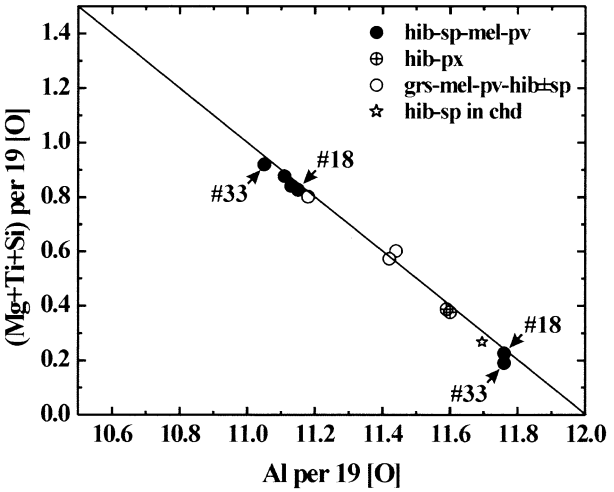

Fig. 13. Concentrations (in atoms per structural formulae calculated based on 19 oxygens) of Al vs. Mg + Ti + Si in hibonite in CAIs from Acfer 094. CAIs 18 and 33 contain both high-Ti and low-Ti hibonites.

The CM CAIs are dominated by spinel-pyroxene assemblages (e.g., MacPherson et al., 1983, 1984), which are rare in Acfer 094. In addition, platy hibonite crystals (PLACs) and spinel-hibonite CAIs (SHIBs) commonly observed in CMs, have not been observed in Acfer 094.

Refractory inclusions in CH chondrites are significantly smaller (~20 μm in apparent diameter) and more refractory on average than those in Acfer 094; grossite- and hibonite-rich CAIs are common, whereas anorthite is virtually absent (e.g., Weber et al., 1995; Krot et al., 2002c; McKeegan et al., 2003), and AOAs are exceptionally rare (Krot, unpublished data).

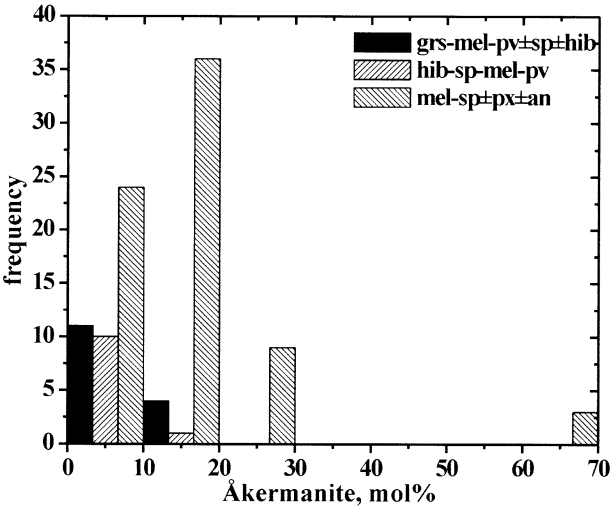

Fig. 14. Histogram of åkermanite (Åk) content (in mol%) in melilite in CAIs from Acfer 094. Åkermanite content increases in the order grossite-bearing → hibonite-bearing → melilite-rich CAIs.

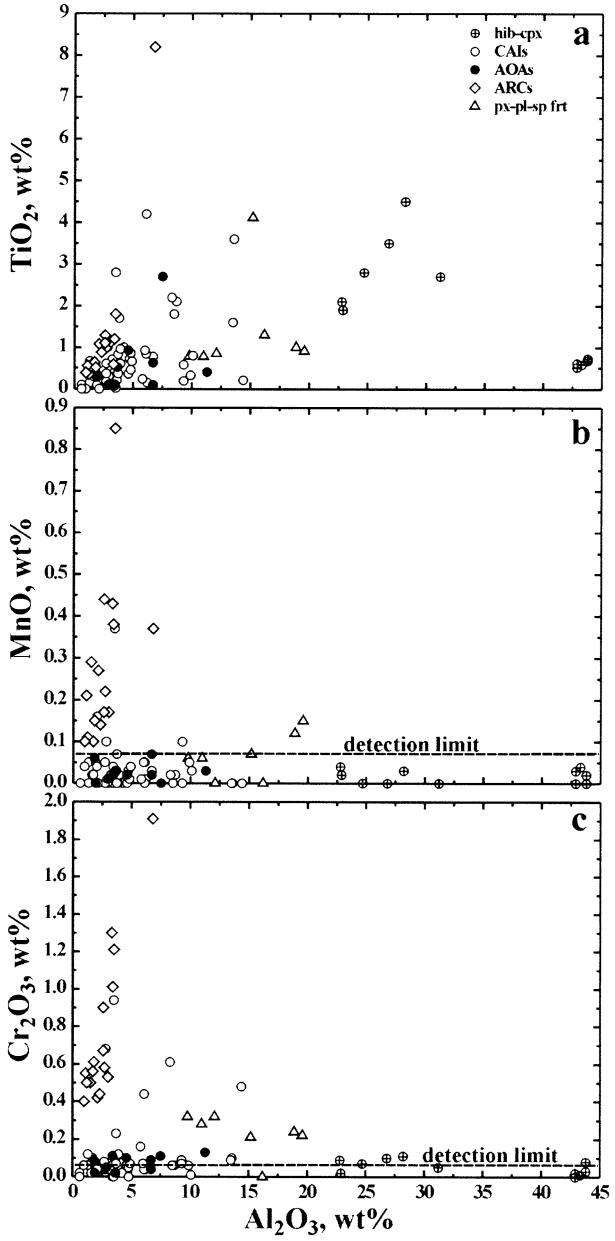

Fig. 15. Concentrations (in wt%) of Al_2O_3 vs. TiO_2 (a), MnO (b) and Cr_2O_3 (c) in high-Ca pyroxenes in CAIs, AOAs, ARCs, and spinel-pyroxene-plagioclase fragments with igneous textures from Acfer 094. High-Ca pyroxenes in ARCs and spinel-pyroxene-plagioclase fragments are enriched in MnO and Cr_2O_3 relative to those in CAIs and AOAs. High-Ca pyroxenes in a hibonite-pyroxene spherule have very high and variable Al_2O_3 contents. Dashed lines in (b) and (c) show detection limits of the microprobe analyses.

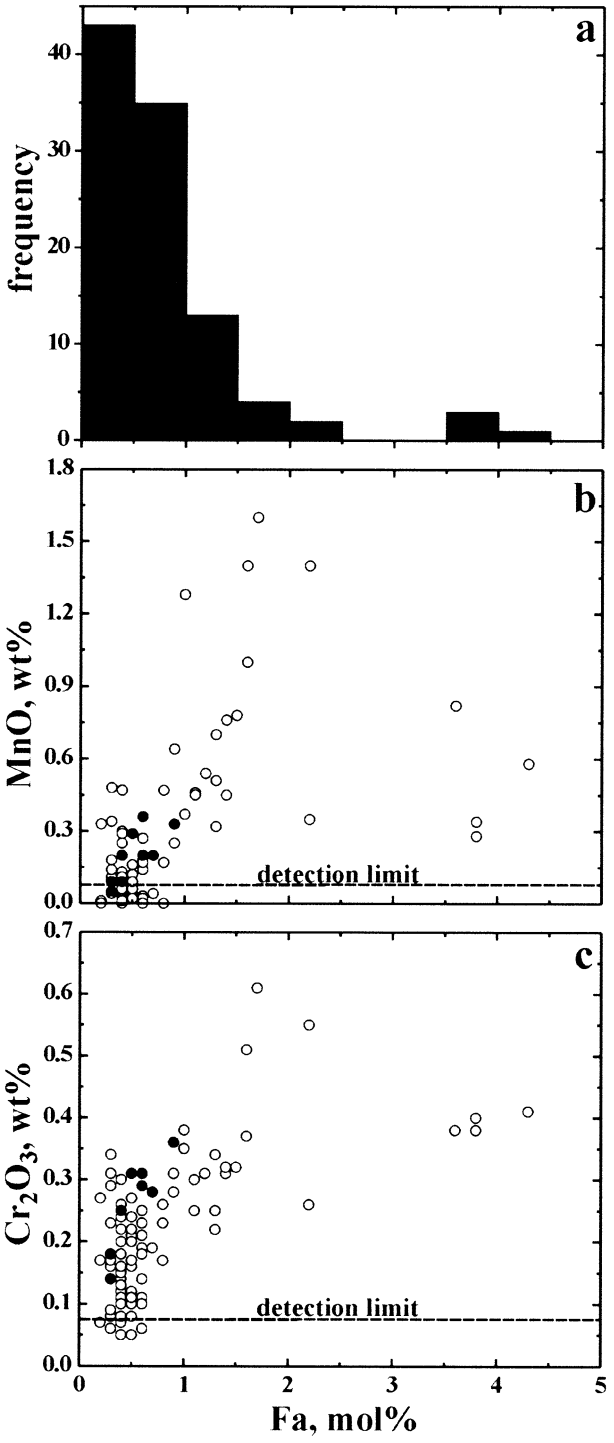

Fig. 16. Histogram (a) of fayalite (Fa) contents (in mol%) and concentrations (in wt%) of MnO (b) and Cr_2O_3 (c) vs. Fa contents in olivine in CAIs (filled symbols) and AOAs (empty symbols) from Acfer 094.

CAIs in CB chondrites are dominantly pyroxene-rich, typically surrounded by monomineralic forsterite rims and contain essentially no anorthite; most CAIs have igneous textures; AOAs are exceptionally rare (Krot et al., 2001a).

Refractory inclusions in CR chondrites are less refractory on average than those in Acfer 094: spinel-pyroxene aggregates, melilite-rich (commonly anorthite-bearing) CAIs, and AOAs are the dominant types; grossite- and hibonite-rich CAIs are rare (Weber and Bischoff, 1997; Aléon et al., 2002).

As a population of objects, refractory inclusions in Acfer 094 are most similar, but not identical, to those in CO chondrites (Weber, 1995; Russell et al., 1998). The grossite- and hibonite-rich CAIs found in Acfer 094 are rare in CO chondrites.

Based on these observations, we infer that refractory inclusions in Acfer 094 form a mineralogically distinct population of

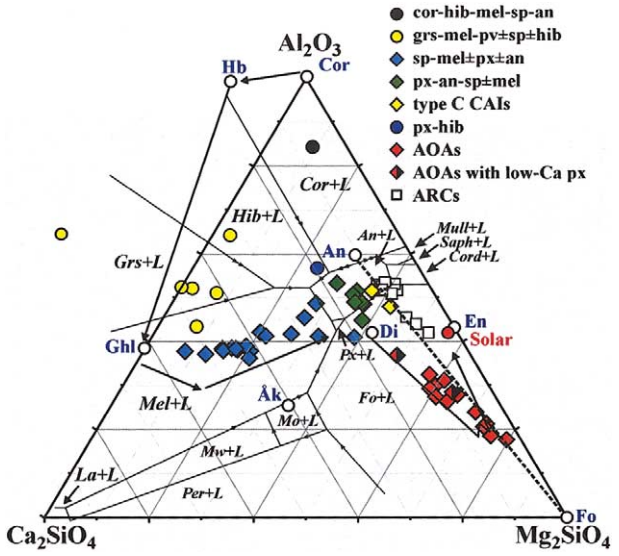

Fig. 17. Bulk compositions of CAIs, AOAs and ARCs from Acfer 094 projected from spinel onto the plane larnite (La)-forsterite (Fo)-corundum (Cor), together with the spinel-saturated liquidus relationships in this system; solid vectors show calculated trajectory for bulk condensed solids during equilibrium condensation (from MacPherson and Huss, 2000). Dashed line connecting anorthite and forsterite is a thermal divide. Bulk compositions of AOAs and CAIs plot to the left from the thermal divide. Bulk compositions of ARCs are similar to pyroxene-anorthite-rich CAIs but plot to the right from the thermal divide.

objects, most similar to that in CO chondrites. The fact that each chondrite group appears to have a distinct population of refractory inclusions may suggest multiple episodes of CAI formation in the nebula, each characterized by a distinct set of physicochemical conditions (Krot et al., 2002c).

4.4. Amoeboid Olivine Aggregates: Origin by Aggregation of Gas-Solid Nebular Condensates

Similar to AOAs from the reduced CV chondrites (Komatsu et al., 2000) and type 3.0 CO chondrites (Chizmadia et al., 2002), AOAs in Acfer 094 are irregularly shaped, porous objects with mineralogy and textures generally consistent with formation as aggregates of gas-solid nebular condensates, such as forsterite and FeNi-metal, and a refractory component composed of Al-diopside, spinel, anorthite, and minor melilite. The refractory minerals in AOAs appear to have recorded similar nebular reactions to those observed in CAIs (reactions 1–4). In addition, forsterite grains in the peripheries of 5 AOAs are replaced by low-Ca pyroxene, suggesting the following reaction:

$$Mg_2SiO_4 + SiO(g) + H_2O(g) = Mg_2Si_2O_6 + H_2(g)\,. \quad (5)$$

Relatively high contents of Al_2O_3 and CaO in these pyroxene may suggest either a small degree of melting of the AOAs or "contamination" of the analyses by submicron-sized inclusions of Al-diopside and anorthite commonly observed as inclusions in forsterite of AOAs (Fig. 6f; Komatsu et al., 2000). If this replacement occurred by a gas-solid reaction, which is kinetically sluggish (Imae et al., 1993), it must have taken place in CAI-forming region characterized by high ambient nebular temperature (>1200–1300 K; Krot et al., 2000d) and ^{16}O-rich isotopic composition (Krot et al., 2002a). If this reaction occurred at subsolidus temperatures, it may have taken place in chondrule-forming regions that generally appear to have ^{16}O-poor isotopic composition (Leshin et al., 1998). Oxygen-isotopic studies of AOAs with low-Ca pyroxene can potentially help to distinguish between these scenarios (e.g., Krot et al., 2004).

4.5. Al-Rich Chondrules: Origin by Melting of a Mixture of Ca,Al-Rich and Ferromagnesian Precursors

The Al-rich chondrules in Acfer 094 are texturally and mineralogically similar to those in CR and reduced CV chondrites (Krot et al., 2002b,c), suggesting similar precursor materials. Many consist of chemically and mineralogically distinct portions: Ca,Al-rich portions largely composed of anorthitic plagioclase, high-Ca pyroxene, and ± spinel, and Fe,Mg-rich portions mainly composed of low-Ca pyroxene, high-Ca pyroxene, forsteritic olivine, FeNi-metal, and glassy or crystalline mesostasis (Figs. 9 and 10). The mineralogy and bulk compositions of the Ca,Al-rich portions are similar to those of Type C and pyroxene-anorthite-rich CAIs from Acfer 094, whereas ferromagnesian portions are mineralogically and chemically similar to Type I chondrules. The heterogeneous Al-rich chondrules probably reflect a heterogeneity in the precursor materials because melting of a homogeneous mixture of aluminous and ferromagnesian grains of appropriate composition would produce a single liquid.

These observations must indicate that the Al-rich chondrules formed by melting of heterogeneous precursor materials composed of mixtures of refractory, Ca,Al-rich components compositionally similar to pyroxene-anorthite-rich CAIs and Fe,Mg-rich components compositionally similar to normal (ferromagnesian) chondrules. According to this model, the Ca,Al-rich portions of the Al-rich chondrules may represent CAIs melted to varying extent during chondrule formation. This interpretation accounts for the heterogeneous Al-rich chondrules, as a relatively large CAI or CAI fragment surrounded by ferromagnesian grains provides a heterogeneity in precursor materials that could result in the observed textures. The presence of some CAIs in chondrule-forming regions before chondrule-formation is supported further by the hibonite-bearing CAI enclosed in a ferromagnesian chondrule (Fig. 8). This model is consistent with the common presence of relict spinel-pyroxene-anorthite-rich CAIs in Al-rich chondrules from the CV, CO, CR, and CH chondrites (Jones and Brearley, 1994; Hutcheon and Jones, 1995; Jones and Hutcheon, 1996; Krot et al., 2000b; Krot and Keil, 2002b). In addition, the presence of a refractory component in precursor materials for the Al-rich chondrules from CO and CV chondrites has been previously inferred from their oxygen isotopic and trace element studies (e.g., Misawa and Nakamura, 1988, 1996; Sheng et al., 1991; Maruyama et al., 1999).

The possible presence[2] of the least refractory, pyroxene-anorthite-spinel CAIs as relict objects inside Al-rich chondrules is consistent with the observed compositional (Fig. 17) and mineralogical evolution (reactions 1–4) of CAIs in Acfer 094,

[2] The relic origin of the Ca, Al-rich portions in the Acfer 094 Al-rich chondrules is inferred so far only from the mineralogical observations; trace element and isotope studies are required to test this hypothesis.

suggesting that Al-diopside, anorthite, and spinel are the final products of this evolution. We note that the bulk compositions of refractory inclusions and AOAs in Acfer 094 plot to the left of the plagioclase-olivine thermal divide, whereas bulk compositions of the Al-rich chondrules plot to the right (Fig. 17). These observations and higher abundances of moderately volatile elements, such as Mn, Cr, and Na, in Al-rich chondrules compared to CAIs and AOAs suggest that simple melting of CAIs or AOAs, without addition of more Si- and volatile-rich material cannot produce Al-rich chondrules. This addition could have occurred either as a result of mixing of CAI-like solids with ferromagnesian precursors rich in Si (e.g., dust of solar composition) and moderately volatile element materials before melting, or by direct condensation of SiO and moderately volatile elements into chondrule melts (Tissandier et al., 2002).

The inferred presence of CAI-like material among the precursors for Al-rich chondrules is in apparent conflict with the lack of evidence for melting of CAIs outside chondrules, suggesting CAIs were largely absent from chondrule-forming region(s) during chondrule formation. This may imply several populations of CAIs in Acfer 094. Mixing of "normal" CAIs (which occur outside chondrules) and chondrules accreting into the Acfer 094 parent asteroid took place after chondrule formation. This hypothesis is generally consistent with the presence of the mineralogically and isotopically unique, hibonite-rich CAI inside chondrule 17. Alternatively, the CAI- and chondrule-forming regions may have overlapped, allowing the least refractory CAIs to mix with Fe,Mg-rich chondrule precursors. This hypothesis, however, is difficult to reconcile with the lack of evidence for melting of AOAs representing aggregates of the least refractory CAIs and forsterite grains.

5. CONCLUSIONS

Refractory inclusions in Acfer 094 can be divided into corundum-rich (0.5%), hibonite-rich (1.1%), grossite-rich (8.5%), spinel-melilite-rich (50.3%), pyroxene-anorthite-rich (7.4%), and Type C (pyroxene-anorthite-rich with igneous textures; 1.6%) Ca,Al-rich inclusions, pyroxene-hibonite spherules (0.5%), and amoeboid olivine aggregates (AOAs, 30.2%).

The mineralogy, textures, and bulk chemistry of these inclusions are consistent with a gas-solid condensation origin and may reflect continuous interaction with SiO and Mg of the cooling nebula gas; only a few CAIs experienced subsequent melting.

None of the CAIs or AOAs show evidence for Fe-alkali metasomatic alteration typical of refractory inclusions in the enstatite, oxidized CV and metamorphosed CO carbonaceous chondrites.

Refractory inclusions in Acfer 094 form a mineralogically distinct population of objects, most similar to that in CO chondrites The fact that each chondrite group appears to have a distinct population of refractory inclusions may suggest that there were multiple episodes of CAI formation in the nebula, each characterized by a distinct set of physical-chemical conditions.

Al-rich chondrules in Acfer 094 are mineralogically similar to those in other carbonaceous chondrite groups (CO, CV, CR) and consist of forsteritic olivine and low-Ca pyroxene phenocrysts, pigeonite, augite, anorthitic plagioclase, FeNi-metal, and crystalline mesostasis composed of plagioclase, augite and a silica phase. Some of the Al-rich chondrules contain Ca,Al-rich portions which appear to be relict, remelted CAIs largely composed of anorthite, high-Ca pyroxene, and spinel. We infer that Al-rich chondrules formed by melting of precursor materials composed of a mixture of a refractory, Ca, Al-rich component compositionally similar to pyroxene-anorthite-rich CAIs and a Fe-Mg component compositionally similar to normal chondrules.

Acknowledgments—We thank Dr. D. Weber and Dr. A. Greshake for providing the polished thin sections of Acfer 094 studied here. This work was supported by NASA grants NAG 5-10610 (A. N. Krot, P.I.), W-19984 (I. Hutcheon, P.I.), NAG5-4704 (K. D. McKeegan, P.I.), and NAG 5-4212 and NAG 5-11591 (K. Keil, P.I.). We thank Dr. H. C. Connolly, Dr. M. K. Weisberg, Dr. M. Grady, and the anonymous reviewer for valuable comments and suggestions. This work was performed under the auspices of the U. S. Department of Energy by the University of California, Lawrence Livermore National Laboratory under Contract No. W-7405-Eng-48. This is Hawaii Institute of Geophysics and Planetology publication No. HIGP 1325 and School of Ocean and Earth Science and Technology publication No. SOEST 6367.

Associate editor: M. Grady

REFERENCES

Aléon J., Krot A. N., and McKeegan K. D. (2002) Ca-Al–rich inclusions and amoeboid olivine aggregates from the CR carbonaceous chondrites. *Meteorit. Planet. Sci.* **37,** 1729–1755.

Beckett J. R. and Stolper E. (1994) The stability of hibonite, melilite and other aluminous phases in silicate melts; implications for the origin of hibonite-bearing inclusions from carbonaceous chondrites. *Meteoritics* **29,** 41–65.

Bischoff A. and Keil K. (1984) Al-rich objects in ordinary chondrites: Related origin of carbonaceous and ordinary chondrites and their constituents. *Geochim. Cosmochim. Acta* **48,** 693–709.

Chizmadia L. J., Rubin A. E., and Wasson J. T. (2002) Mineralogy and petrology of amoeboid olivine inclusions in CO3 chondrites: Relationship to parent-body aqueous alteration. *Meteorit. Planet. Sci.* **37,** 1781–1797.

Connolly H. C., Jr. and Burnett D. S. (1999) A study of the minor element concentrations of spinels from two type B calcium-aluminum-rich inclusions; an investigation into potential formation conditions of calcium-aluminum-rich inclusions. *Meteorit. Planet. Sci.* **34,** 829–848.

Ebel D. S. and Grossman L. (2000) Condensation in dust-enriched systems. *Geochim. Cosmochim. Acta* **64,** 339–366.

Fagan T. J., Krot A. N., and Keil K. (2000) Calcium,. Aluminum-rich inclusions in enstatite chondrites. *Meteorit. Planet. Sci.* **35,** 771–783.

Fagan T. J., Krot A. N., and Yurimoto H. (2003) Petrology and oxygen isotope compositions of refractory inclusions from Acfer 094 (abstract). *Lunar Planet. Sci.* **34,** 1274.

Gao X., Amari S., Messenger S., Nittler L. R., Swan P. D., and Walker R. M. (1996) Survey of circumstellar grains in the unique carbonaceous chondrite Acfer 094 (abstract). *Meteorit. Planet. Sci.* **31,** A48.

Greshake A. (1997) The primitive matrix components of the unique carbonaceous chondrite Acfer 094; a TEM study. *Geochim. Cosmochim. Acta* **61,** 437–452.

Grossman L. and Steele I. M. (1976) Amoeboid olivine aggregates in the Allende meteorite. *Geochim. Cosmochim. Acta* **40,** 149–155.

Hsu W., Wasserburg G. J., and Huss G. R. (2000) High time resolution by use of the ^{26}Al chronometer in the multistage formation of a CAI. *Earth Planet. Sci. Lett.* **182,** 15–29.

Huss G. R., Hutcheon I. D., Krot A. N., and Tachibana S. (2003) Oxygen isotopes in refractory inclusions from the Adelaide carbonaceous chondrite (abstract). *Lunar Planet. Sci.* **34,** 1802.

Hutcheon I. D. and Jones R. H. (1995) The ^{26}Al-^{26}Mg record of chondrules: Clues to nebular chronology (abstract). *Lunar Planet. Sci.* **26,** 647–648.

Hutcheon I. D., Krot A. N., and Ulyanov A. A. (2000) ^{26}Al in anorthite-rich chondrules in primitive carbonaceous chondrites: Ev-

idence chondrules post-date CAI (abstract). *Lunar Planet. Sci.* **31,** 1869.

Imae N., Tsuchiyama A., and Kitamura M. (1993) An experimental study of enstatite formation reaction between forsterite and Si-rich gas. *Earth Planet. Sci. Lett.* **118,** 21–30.

Jones R. H. and Brearley A. (1994) Reduced, plagioclase-rich chondrules in the Lance and Kainsaz CO3 chondrites (abstract). *Lunar Planet. Sci.* **25,** 641–642.

Jones R. H. and Hutcheon I. D. (1996) Mineralogy and secondary alteration of a complex plagioclase-rich inclusion in Kainsaz (abstract). *Meteorit. Planet. Sci.* **31,** 67–68.

Kimura M. and Ikeda Y. (1997) Comparative study of anhydrous alteration of chondrules in reduced and oxidized CV chondrites. *Proc. NIPR Symp. Antarct. Meteorit.* **10,** 191–202.

Komatsu M., Krot A. N., Petaev M. I., Ulyanov A. A., Keil K., and Miyamoto M. (2000) Mineralogy and petrography of amoeboid olivine aggregates from the reduced CV3 chondrites Efremovka, Leoville and Vigarano: Products of nebular condensation and accretion. *Meteorit. Planet. Sci.* **36,** 629–643.

Krot A. N., Scott E. R. D., and Zolensky M. E. (1995) Mineralogic and chemical variations among CV3 chondrites and their components: Nebular and asteroidal processing. *Meteoritics* **30,** 748–775.

Krot A. N., Petaev M. I., Scott E. R. D., Choi B.-G., Zolensky M. E., and Keil K. (1998) Progressive alteration in CV3 chondrites: More evidence for asteroidal alteration. *Meteorit. Planet. Sci.* **33,** 1065–1085.

Krot A. N., Sahijpal S., McKeegan K. D., Weber D., Greshake A., Ulyanov A. A., Hutcheon I. D., and Keil K. (1999) Mineralogy, aluminum-magnesium and oxygen isotope studies of the relic calcium-aluminum-rich inclusions in chondrules (abstract). *Meteorit. Planet. Sci.* **34,** A68–A69.

Krot A. N., McKeegan K. D., Russell S. S., Meibom A., Weisberg M. K., Zipfel J., Krot T. V., Fagan T. J., and Keil K. (2001a) Refractory Ca,Al-rich inclusions and Al-diopside-rich chondrules in the metal-rich chondrites Hammadah al Hamra 237 and QUE 94411. *Meteorit. Planet. Sci.* **36,** 1189–1217.

Krot A. N., Huss G. R., and Hutcheon I. D. (2001b) Corundum-hibonite refractory inclusions from Adelaide: Condensation or crystallization from melt? (abstract). *Meteorit. Planet. Sci* **36 (***Suppl***),** A105.

Krot A. N., Huss G. R., and Hutcheon I. D. (2001c) Aluminum-rich chondrules and associated refractory inclusions in the unique carbonaceous chondrite Adelaide (abstract). *Meteorit. Planet. Sci* **36 (***Suppl.***),** A105–A106.

Krot A. N. and Keil K. (2002) Anorthite-rich chondrules in CR and CH carbonaceous chondrites: Genetic link between Ca,Al-rich inclusions and ferromagnesian chondrules. *Meteorit. Planet. Sci.* **37,** 91–111.

Krot A. N., McKeegan K. D., Leshin L. A., MacPherson G. J., and Scott E. R. D. (2002a) Existence of an ^{16}O-rich gaseous reservoir in the solar nebula. *Science* **295,** 1051–1054.

Krot A. N., Hutcheon I. D., and Keil K. (2002b) Anorthite-rich chondrules in the reduced CV chondrites: Evidence for complex formation history and genetic links between CAIs and ferromagnesian chondrules. *Meteorit. Planet. Sci.* **37,** 155–182.

Krot A. N., Meibom A., Weisberg M. K., and Keil K. (2002c) The CR chondrite clan: Implications for early solar system processes. *Meteorit. Planet. Sci.* **37,** 1451–1490.

Krot A. N., MacPherson G. J., Ulyanov A. A. and Petaev M. I. (2003a) Fine-grained, spinel-rich inclusions from the reduced CV chondrites Efremovka and Leoville: I. Mineralogy, petrology and bulk chemistry. *Meteorit. Planet. Sci.*, submitted.

Krot A. N., Petaev M. I., and Yurimoto H. (2004) Amoeboid olivine aggregates with low-Ca pyroxenes: a genetic link between refractory inclusions and chondrules? *Geochim. Cosmochim. Acta* **68**(7)**,** 1923–1941.

Kurat G. and Kracher A. (1980) Basalts in the Lance carbonaceous chondrite. *Zeitschr. Naturforsch.* **35A,** 180–190.

Leshin L. A., McKeegan K. D., Engrand C., Zanda B., Bourot-Denise M., and HeWins R. H. (1998) Oxygen-isotopic studies of isolated and chondrule olivine from Renazzo and Allende (abstract). *Meteorit. Planet. Sci.* **33,** A93–A94.

Lee M. R. and Greenwood R. C. (1994) Alteration of calcium- and aluminum-rich inclusions in the Murray (CM2) carbonaceous chondrite. *Meteoritics.* **29,** 780–790.

MacPherson G. J., Bar-Matthews M., Tanaka T., Olsen E., and Grossman L. (1983) Refractory inclusions in the Murchison meteorite. *Geochim. Cosmochim. Acta* **47,** 823–840.

MacPherson G. J., Grossman L., Hashimoto A., Bar-Matthews M., and Tanaka T. (1984) Petrographic studies of refractory inclusions from the Murchison meteorite. *J. Geophys. Res.* **89,** C299–C312.

MacPherson G. J., Wark D. A., and Armstrong J. T. (1988) Primitive material surviving in chondrites: Refractory inclusions. In *Meteorites and the Early Solar System* (eds. F. Kerridge and M. S. Matthews), pp. 746–807. University of Arizona Press.

MacPherson G. J. and Davis A. M. (1993) A petrologic and ion microprobe study of a Vigarano type B refractory inclusion; evolution by multiple stages of alteration and melting. *Geochim. Cosmochim. Acta* **57,** 231–243.

MacPherson G. J. and Huss G. R. (2000) Convergent evolution of CAIs and chondrules: Evidence from bulk compositions and a cosmochemical phase diagram (abstract). *Lunar Planet. Sci.* **31,** 1796.

MacPherson G. J., Krot, A. N., Ulyanov, A. A., and Hicks, T (2002) A comprehensive study of pristine, fine-grained, spinel-rich inclusions from the Leoville and Efremovka CV3 chondrites, I: Petrology (abstract). *Lunar Planet. Sci.* **33,** #1526.

Maruyama S., Yurimoto H., and Sueno S. (1999) Oxygen isotope evidence regarding the formation of spinel-bearing chondrules. *Earth Planet. Sci. Lett.* **169,** 165–171.

Misawa K. and Nakamura N. (1988) Highly fractionated rare-earth elements in ferromagnesian chondrules from the Felix (CO3) meteorite. *Nature* **334,** 47–49.

Misawa K. and Nakamura N. (1996) Origin of refractory precursor components of chondrules from carbonaceous chondrites. In *Chondrules and the Protoplanetary Disk* (eds. Hewins R. H., Jones R. H. and Scott E. R. D.), pp. 99–105. Cambridge Univ. Press.

Newton J., Bischoff A., Arden J. W., Franci I. A., Geriger T., Greshake A., and Pillinger C. T. (1995) Acfer 094, a uniquely primitive carbonaceous chondrite from the Sahara. *Meteoritics* **30,** 47–56.

Petaev M. I. and Wood J. T. (1998) The condensation with partial isolation (CWPI) model of condensation in the solar nebula. *Meteorit. Planet. Sci.* **33,** 1123–1137.

Petaev M. I., Wood J. A., Meibom A., Krot A. N., and Keil K. (2003) The ZONMET thermodynamic and kinetic model of metal condensation. *Geochim. Cosmochim. Acta* **67,** 1737–1751.

Russell S. S., Huss G. R., Fahey A. J., Greenwood R. C., Hutchison R., and Wasserburg G. J. (1998) An isotopic and petrologic study of calcium-aluminum-rich inclusions from CO3 chondrites. *Geochim. Cosmochim. Acta* **62,** 689–714.

Sahijpal S., McKeegan K. D., Krot A. N., Weber D. C., Ulyanov A. A. (1999) Oxygen isotopic compositions of calcium-aluminum-rich inclusions from the CH chondrites, Acfer 182 and PAT91546 (abstract). *Meteorit. Planet. Sci.* **34,** A101.

Sheng Y. J., Hutcheon I. D., and Wasserburg G. J. (1991) Origin of plagioclase-olivine inclusions in carbonaceous chondrites. *Geochim. Cosmochim. Acta* **55,** 581–599.

Tissandier L., Libourel G., and Robert F. (2002) Gas-melt interactions and their bearings on chondrule formation. *Meteorit. Planet. Sci.* **37,** 1377–1389.

Weber D. (1995) Refractory inclusions from the carbonaceous chondrite Acfer 094 (abstract). *Meteoritics* **30,** 595–596.

Weber D., Zinner E., and Bischoff A. (1995) Trace element abundances and magnesium, calcium, and titanium isotopic compositions of grossite-containing inclusions from the carbonaceous chondrite Acfer 182. *Geochim. Cosmochim. Acta* **59,** 803–823.

Weber D. and Bischoff A. (1997) Refractory inclusions in the CR chondrite Acfer 059–El Djouf 001: Petrology, chemical composition, and relationship to inclusion populations in other types of carbonaceous chondrites. *Chem. Erde.* **57,** 1–24.

Yoneda S. and Grossman L. (1995) Condensation of CaO-MgO-Al_2O_3-SiO_2 liquids from cosmic gases. *Geochim. Cosmochim. Acta* **59,** 3413–3444.

Yurimoto H., Nagasawa H., Mori Y., and Matsubaya O. (1994) Microdistribution of oxygen isotopes in a refractory inclusion from the Allende meteorite. *Earth Planet. Sci. Lett.* **128,** 47–53.

Yurimoto H., Ito M., and Nagasawa H. (1998) Oxygen isotope exchange between refractory inclusion in Allende and solar nebula gas. *Science* **282,** 1874–1877.